Behind the Horizon of the Charged Anti-de Sitter Black Hole

by

JIANYANG HE

A THESIS SUBMITTED IN PARTIAL FULFILMENT OF
THE REQUIREMENTS FOR THE DEGREE OF

Master of Science

in

The Faculty of Graduate Studies

(Physics)

The University Of British Columbia

April 20, 2005

Abstract

There is a correspondence between the supergravity in $AdS_5 \times S^5$ space and $\mathcal{N} = 4$ super-Yang-Mills theory. In this sense, we study the region inside the event horizon of charged black holes in five dimensional asymptotically anti-de Sitter space, using the two-point correlation functions dominated by the spacelike geodesics between the operators at different sides of the asymptotical boundary. With some null perturbation, we find the spacetime structure is changed, as well as the correlation functions, providing a method of scanning the region between inner and out horizons. Surprisingly, the two-sided correlators we calculate seem to be geometrically protected from the instability of the inner horizon.

Contents

List of Figures

Preface

This is my second Master thesis, and maybe my last work in physics.

Acknowledgements

Thanks to Moshe. As my supervisor, he helps me so much, from the ideas of our work, to the details of the calculation. And gave me the chance to work in string theory with general relativity, which I really wanted to know. Also coming with him to Perimeter institute is very important to me, with so many opportunities to communicate with the other physicists. The talks in almost everyday make me more familiar with the processes in string theory. As a master student, I was supported by Moshe for the whole term in PI, without any TA responsibility. It is a very few case in general. In a word, he is a very very nice person. I am very happy to have been doing work with him.

Mark: My advisor of the course EM. A very nice and popular guy. I like his classes, which is clear and heuristic. And it was a good experience to be TA of his course. Unfortunately, he is too popular that I have not much chance to ask him many questions.

Dom: My coworker. Actually I should not use this word, since he know much more than I and helped me a lot. Especially in GR and maple calculation, with his help I finally knew how to use them. A nice English man, I like his British accent.

Callum: Both supervised by Moshe, we usually discussed together. He has a good physics tuition and often gives some illuminating ideas. In the life in Waterloo, he did almost everything for our living, and helped me about the accommodation in Toronto. Many Thanks, my roommate.

Thanks to Perimeter Institute, where I spent my last term in Canada and wrote my thesis. It is a very good place for theoretical physicists, hospitable and providing so many opportunities of talks and conferences.

It seems a big list to which I should show my appreciation. Brian, a polite Chinese, always does his best to help others. Tony, almost the first Canadian when I came here, is very nice and helpful. What a pity that he will leave the department this term. Janis, Lydia, ...

I should appreciate my mother and family's kindness of allowing me to do whatever I want since I was only a teenager. Even I fail in my work, I am not failing in my life and will never regret my choice.

The last and most important thank is to my girlfriend, Fanshan, who waited for me for long time, backing me up all the time. It is the time for me to do something for her now. I love her.

Chapter 1

Introduction

AdS/CFT correspondence is the most important work in recent years in string theory[1, 2], with a good review as [3] and a new important work [4]. It gives a description of the duality between 10 dimensional supergravity and 4 dimensional gauge theory, which gives a new way of reducing from 10d string theory to 4d field theory and makes us more confident that string theory may be really "the theory of everything" we want. In the well known case, the supergravity in $AdS_5 \times S^5$ is identical with $\mathcal{N} = 4$ super-Yang-Mills theory, which we can solve from the low energy limit of 10d string theory and D-brane theory.

In a classical black hole, everything just can enter the horizon, but cannot get out from inner region. Even Hawking radiation with quantum theory, which mostly comes from the near horizon spacetime and is determined by the basic properties of the black hole, eg. mass and temperature, is considered, it is still difficult to get a well description of deep region behind horizon. Some early efforts are [5, 6, 7, 8]. However AdS/CFT correspondence gives a new way to investigate such a problem. Using the ideas introduced in [11] and further developed in [9, 12, 13, 14, 15, 16, 17], we study the observables which depend on the physics behind the horizon. For an AdS_{p+2} ($p > 1$) black hole, there are two sides of boundary in its Penrose diagram, so it is possible to have the spacelike geodesics crossing the horizons and the inner region. And from the AdS/CFT correspondence we know such geodesics give crucial contribution to correlation functions, the observables in the dual gauge theory.

As discussed in [26], duality exists between the concepts of the thermofield formalism of field theory and black hole physics. The fictitious Hilbert space in the thermofield formalism is just the space of states behind the event horizon of the eternal black hole. By tracing over the fictitious states, we recover the thermal behavior of the physical states. In the AdS version, correlators of operators on one single boundary is the ordinary thermal correlation functions. For the ones between operators inserted on different boundaries, we can use the usual formalism, with a shifting of the time by half of the period [9, 11].

Following this idea, Schwarzschild black hole in AdS_5 space was investigated in [9]. In that work, the authors showed the Penrose diagram in the beginning, as well as the causal structure. In calculating the proper length of the symmetric spacelike geodesics, they found a t_c singularity, which gave a contradiction with gauge theory. Then they analytically continue the discussion to complex coordinates, and showed the singularity can be eliminated by the dominance of complex geodesics and therefore there is no singularity in the correlators in gauge theory.

In our work[10], we explore the physics of the charged black holes in AdS_5 space. In a similar way, we give the causal structure and consider a neutral probe particle and then a charged probe particle. Different from Schwarzschild case, the complex geodesics are generally dominated by the real ones, so there is no such singularity in the calculation of

correlation functions. In addition, we turn on a null outgoing perturbation. By tuning the time of the perturbation leaving from the left-hand side boundary, we get a method to scan the region between Cauchy horizons and event horizons. An important and natural result is whatever we do, the inner region behind Cauchy horizons is never reached, which verifies the cosmic censorship principle [18].

The outline of the thesis is as following. In chapter 2, we review some background knowledge, including conformal field theory, AdS space and thermal field theory[19], as well as a simple description of the AdS/CFT correspondence. Then we give a summary of the work on Schwarzschild AdS black hole in chapter 3. The last part, chapter 4 is our work about charged black hole in AdS space.

Chapter 2

Background: AdS, CFT and the Correspondence

2.1 Conformal Field Theory

Symmetry plays a crucial role in modern physics. Our most familiar groups maybe are Lorentz group and Poincaré group. And another important example is scale invariance which links physics in different scales. A scale invariant theory is 4 dimensional Yang-Mills theory. Generally such a scale-invariance cannot be extended to quantum theory, whose definition requires a cutoff apparently breaking the scale invariance. However there is some special cases, eg. 4 dimensional $\mathcal{N} = 4$ Super-Yang-Mills theory.

It is realized that generally in field theory there exist renormalization group flows from scale invariant UV fixed points to IR fixed points, as well as in statistics mechanics there are usually nontrivial IR scale-invariant fixed points. So studying scale-invariant property is interesting and useful in various physics fields.

Conformal Group and Algebra

Conformal group is the transformation preserving the metric with an arbitrary scale factor, $g_{\mu\nu}(x) \to \Omega^2(x) g_{\mu\nu}(x)$, where $\mu, \nu = 0, \cdots, d-1$. It is the minimal group containing Poincaré group and inversion symmetry, $x^\mu \to x^\mu / x^2$. The conformal group in Minkowski space is generated by Poincaré group, scale transformation,

$$x^\mu \to \lambda x^\mu \tag{2.1}$$

and special conformal transformation,

$$x^\mu \to \frac{x^\mu + a^\mu x^2}{1 + 2x^\nu a_\nu + a^2 x^2.} \tag{2.2}$$

The generators are Lorentzian $M_{\mu\nu}$, translation P_μ, scale transformation D, and special conformal transformation K_μ. The conformal algebra are

$$[M_{\mu\nu}, P_\rho] = -i(\eta_{\mu\rho} P_\nu - \eta_{\nu\rho} P_\mu); \qquad [M_{\mu\nu}, K_\rho] = -i(\eta_{\mu\rho} K_\nu - \eta_{\nu\rho} K_\mu);$$
$$[M_{\mu\nu}, M_{\rho\sigma}] = -i\eta_{\mu\rho} M_{\nu\sigma} \pm \text{permutations}; \qquad [M_{\mu\nu}, D] = 0; \qquad [D, K_\mu] = -iK_\mu; \tag{2.3}$$
$$[D, P_\mu] = -iP_\mu; \qquad [P_\mu, K_\nu] = 2iM_{\mu\nu} - 2i\eta_{\mu\nu} D, \tag{2.4}$$

with all the other commutations vanish. This algebra is isometric to the algebra of $SO(d,2)$ with signature $(-,+,+,...,+,-)$ and generators J_{ab} (a,b=0,..., d+1),

$$J_{\mu\nu} = M_{\mu\nu}; \qquad J_{\mu d} = \frac{1}{2}(K_\mu - P_\mu); \qquad J_{\mu(d+1)} = \frac{1}{2}(K_\mu + P_\mu); \qquad J_{(d+1)d} = D. \quad (2.5)$$

Primary Fields, Correlation functions

An interesting representation of conformal group includes some operators which are eigenfunctions of scale transformation, with eigenvalue $-i\Delta$, where Δ is called scaling dimension. That means the operators transform as $\phi(x) \to \phi'(x) = \lambda^\Delta \phi(x)$. We can prove that the operators P_μ raise dimension of the field, while K_μ lower the dimension. Actually there is a lower bound of the scaling dimension, eg. $\Delta \geq (d-2)/2$ for a free scalar field. So there must be some fields with the lowest dimension, called primary fields, which are annihilated by K_μ (at $x = 0$). The action of conformal generators on such operators is

$$\begin{aligned} [P_\mu, \Phi(x)] &= i\partial_\mu \Phi(x), \\ [M_{\mu\nu}, \Phi(x)] &= [i(x_\mu \partial_\nu - x_\nu \partial_\mu) + \Sigma_{\mu\nu}]\Phi(x), \\ [D, \Phi(x)] &= i(-\Delta + x^\mu \partial_\mu)\Phi(x), \\ [K_\mu, \Phi(x)] &= [i(x^2\partial_\mu - 2x_\mu x^\nu \partial_\nu + 2x_\mu \Delta) - 2x^\nu \Sigma_{\mu\nu}]\Phi(x). \end{aligned} \quad (2.6)$$

where $\Sigma_{\mu\nu}$ are the matrices of a finite dimensional Lorentzian group. Here $\Sigma_{\mu\nu}$ and Δ are Casimirs of the conformal group, classifying primary operators.

Another representation of conformal group is the maximal compact subgroup, $SO(d) \times SO(2)$, with $J_{0(d+1)} = \frac{1}{2}(K_0 + P_0)$ as the generator of $SO(2)$. The representation shown in the first way can be decomposed into representations in this subgroup.

As the conformal group includes Poincaré group, there are more restrictions on correlation functions. It can be easily shown that the 2-point functions of different dimensional fields vanish. For a scalar field $\phi(x)$ with scaling dimension Δ,

$$\langle \phi(0)\phi(x) \rangle \propto \frac{1}{|x|^{2\Delta}} \equiv \frac{1}{(x^2)^\Delta}. \quad (2.7)$$

3-point functions are with the form

$$\langle \phi_i(x_1)\phi_j(x_2)\phi_k(x_3) \rangle = \frac{c_{ijk}}{|x_1 - x_2|^{\Delta_1+\Delta_2-\Delta_3}|x_1 - x_3|^{\Delta_1+\Delta_3-\Delta_2}|x_2 - x_3|^{\Delta_2+\Delta_3-\Delta_1}}. \quad (2.8)$$

Similar expressions can be written for 4-point functions, however they can be decomposed into a combination of 3-point functions, as well as for higher n-point functions.

A general property of local field theory is *operator product expansion* (OPE). When we bring two operators $\mathcal{O}_1(x)$ and $\mathcal{O}_2(y)$ to the same point, the product of them can be expanded as sum of other local operators, $\mathcal{O}_1(x)\mathcal{O}_2(y) \to \Sigma_n C_{12}^n(x-y)\mathcal{O}_n(y)$, which can be understood as in correlation functions. In conformal theory, the coefficients can be written as $C_{12}^n(x-y) = c_{12}^n/|x-y|^{\Delta_1+\Delta_2-\Delta_n}$. The leading term in OPE of energy-momentum tensor

is determined by conformal algebra, eg. for a scalar primary field ϕ,

$$T_{\mu\nu}(x)\phi(0) \propto \Delta\phi(0)\partial_\mu\partial_\nu(\frac{1}{x^2}) + \cdots. \tag{2.9}$$

Another important property is the correspondence between local operators $\mathcal{O}$ and states $|\mathcal{O}\rangle$ in the radial quantization of the theory. Taking time coordinate as the radius direction, the origin relates to the initial time or past infinity, and the field theory lives on $\mathbb{R} \times S^{d-1}$. The Hamiltonian in this case is $J_{0(d+1)}$. An operator $\mathcal{O}$ can be mapped to the state $|\mathcal{O}\rangle = \lim_{x\to 0}\mathcal{O}(x)$, which can also be equivalently viewed as a functional of a ball around the origin with the insertion of an operator $\mathcal{O}$ at the origin.

Superconformal algebra and Field theories

It is interesting to add supersymmetry to conformal group, and it was shown that in some dimensions and for some number of supercharges the superconformal group is the largest possible simple algebra including Poincaré group. Superconformal algebras exist only for $d \leq 6$, which restricts our extension of the theories. In addition to the generators of conformal algebra and supersymmetry, we have two more kinds, one is fermionic generators S(one for each supersymmetry generator, usually called super-special conformal generator) which arises from the commutation of K and Q, and the other one is R-symmetry generators R forming some Lie algebra. The internal R-symmetry gives a $U(N)$ algebra, including $SU(N)$ generators T_r and A for $U(1)$ subalgebra. The commutation relations of them are shown below,

$$\begin{array}{llll} [D,Q] = -\frac{i}{2}Q; & [D,S] = \frac{i}{2}S; & [K,Q] \simeq S; & [P,S] \simeq Q; \\ \{Q,Q\} \simeq P; & \{S,S\} \simeq K; & \{Q,S\} \simeq M + D + R, & \\ [Q,T_r] \simeq (1+\gamma_5)Q, & [S,T_r] \simeq (1-\gamma_5)S, & [Q,A] \simeq Q, & [S,A] \simeq -S. \end{array} \tag{2.10}$$

Now let us consider superconformal field theories. The maximal number of supercharges in a free field theory without gravity is 16, and the maximal possible number is the same in an interacting theory, so there are at most 32 fermionic generators in a superconformal field theory. Such number of supercharges are just exist in d =3, 4 or 6. Especially for $d = 4$, the R-symmetry group is $SU(4)$ and the fermionic generators are in the $(4,4)+(\bar{4},\bar{4})$ of $SO(4,2) \times SU(4)$.

For a superconformal algebra, there exist some primary fields, which are annihilated by K_μ and S, and the different primaries of which arise by the supercharges Q. The superconformal algebra has special representations, called as chiral primary operators, which are annihilated by some combination of supercharges. The dimension of such chiral primary operators is determined by their R-symmetry representations and cannot receive any quantum corrections. For the non-chiral primary fields, the dimensions are always strictly larger than those of chiral primary fields.

2.2 Anti-de Sitter Space

Conformal Structure of Flat Space

For a general Minkowski space $R^{1,p}$ $(p \geq 2)$,

$$ds^2 = -dt^2 + dr^2 + r^2 d\Omega_{p-1}^2, \tag{2.11}$$

where $d\Omega_{p-1}^2$ is the element of S^{p-1}.

We can make a series of coordinate transformations as,

$$\begin{aligned} ds^2 &= -du_+ du_- + \frac{1}{4}(u_+ - u_-)^2 d\Omega_{p-1}^2, && (u_\pm = t \pm r) \\ &= \frac{1}{\cos^2 \tilde{u}_+ \cos^2 \tilde{u}_-} \left(-d\tilde{u}_+ d\tilde{u}_- + \frac{1}{4} \sin^2(\tilde{u}_+ - \tilde{u}_-) d\Omega_{p-1}^2 \right), && (u_\pm = \tan \tilde{u}_\pm) \\ &= \frac{1}{4 \cos^2 \tilde{u}_+ \cos^2 \tilde{u}_-} (-d\tau^2 + d\theta^2 + \sin^2 \theta d\Omega_{p-1}^2), && (\tilde{u}_\pm = (t \pm \theta)/2) \end{aligned} \tag{2.12}$$

The conformal structure of $R^{1,p}$ is shown as a triangular region in figure 2.1. If we just consider the causal structure, the metric can be analytically continued to the whole (τ, θ) plane, with a conformally scaled metric

$$ds'^2 = -d\tau^2 + d\theta^2 + \sin^2 \theta d\Omega_{p-1}^2, \tag{2.13}$$

where

$$0 \leq \theta \leq \pi, \qquad -\infty < \tau < +\infty. \tag{2.14}$$

Obviously such a region has the geometry of $\mathbb{R} \times S^p$(Einstein static universe), with $\theta = 0$ and π relate to the north and south pole of S^p.

Anti-de Sitter Space

The $(p+2)$-dimensional AdS space (AdS_{p+2}) is described as a hyperboid

$$X_0^2 + X_{p+2}^2 - \sum_{i=1}^{p+1} X_i^2 = R^2, \tag{2.15}$$

which is embedded in $(p+3)$ dimensional space with metric

$$ds^2 = -dX_0^2 - dX_{p+2}^2 + \sum_{i=1}^{p+1} dX_i^2. \tag{2.16}$$

We can make the coordinate transformation as

$$\begin{aligned} X_0 &= R \cosh \rho \cos \tau, \qquad X_{p+2} = R \cosh \rho \sin \tau, \\ X_i &= R \sinh \rho \Omega_i \qquad (i = 1, \cdots, p+1; \sum_i \Omega_i^2 = 1), \end{aligned} \tag{2.17}$$

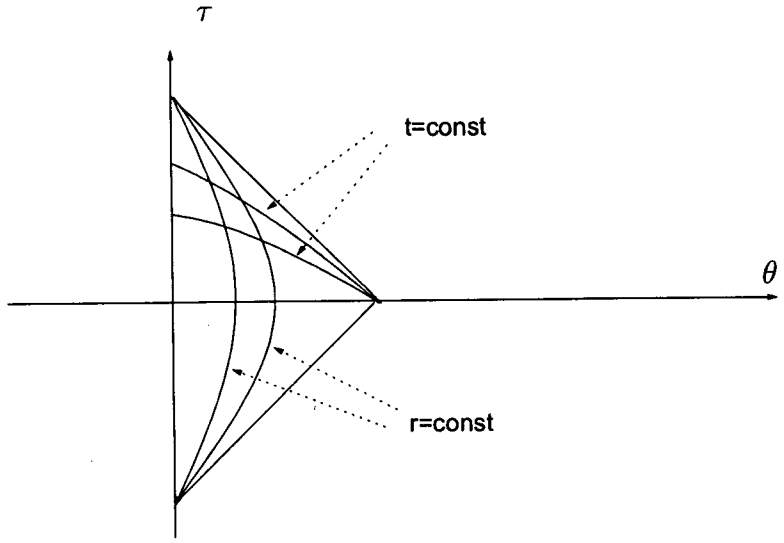

Figure 2.1: **The conformal structure of $R^{1,p}$ Minkowski space.**

and the metric is changed to

$$\mathrm{d}s^2 = R^2(-\cosh^2\rho\ \mathrm{d}\tau^2 + \mathrm{d}\rho^2 + \sinh^2\rho\ \mathrm{d}\Omega^2). \tag{2.18}$$

Setting $\tan\theta = \sinh\rho (0 \leq \theta < \pi/2)$, it transfers to

$$\mathrm{d}s^2 = \frac{R^2}{\cos^2\theta}(-\mathrm{d}\tau^2 + \mathrm{d}\theta^2 + \sin^2\theta \mathrm{d}\Omega^2). \tag{2.19}$$

The causal structure will not changed when we do a conformal transformation, so it is the same as

$$\mathrm{d}s'^2 = -\mathrm{d}\tau^2 + \mathrm{d}\theta^2 + \sin^2\theta \mathrm{d}\Omega^2. \tag{2.20}$$

This is Einstein static universe, the same as in equation (2.13). However, the value region of θ here is $0 \leq \theta < \pi/2$, instead of $0 \leq \theta < \pi$ as in (2.13), so the AdS_{p+2} can be conformally mapped into half of Einstein static universe. Figure 2.2 shows the special example AdS_3. In general, if a spacetime can be conformally mapped into half of Einstein static universe, it is called asymptotically AdS. The boundary of conformally compactified AdS_{p+2} is identical to the boundary of conformal compactification of (p+1) dimensional Minkowski spacetime, which is the key of the correspondence between AdS_{p+2} and CFT_{p+1}.

There is another very useful coordinate system of AdS. From equation (2.16), we set

$$\begin{aligned} X_0 &= \frac{1}{2u}\left(1 + u^2(R^2 + \vec{x}^2 - t^2)\right), \qquad X_{p+2} = Rut, \\ X^i &= Rux^i \quad (i = 1, \cdots, p), \end{aligned}$$

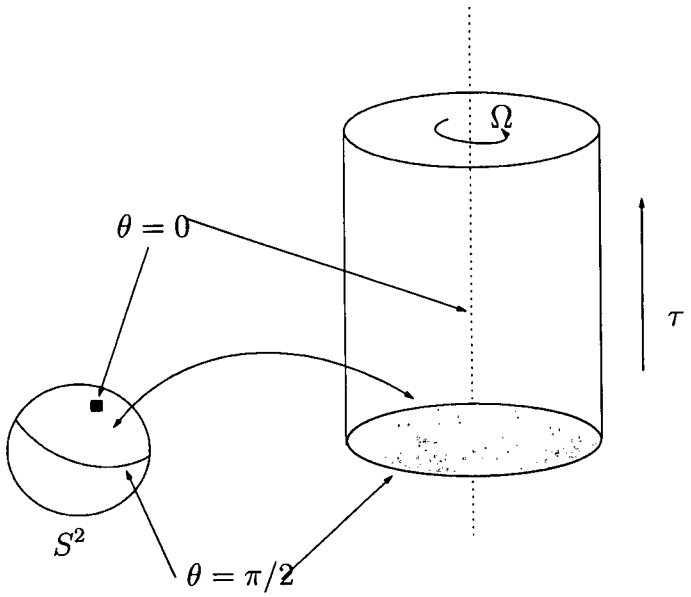

Figure 2.2: **The conformal structure of Anti-de Sitter 3 dimensional space.**

$$X^{p+1} = \frac{1}{2u}\left(1 - u^2(R^2 - \vec{x}^2 + t^2)\right). \tag{2.21}$$

The metric is now

$$\mathrm{d}s^2 = \left(\frac{\mathrm{d}u^2}{u^2} + u^2(-\mathrm{d}t^2 + \mathrm{d}\vec{x}^2)\right). \tag{2.22}$$

The coordinates $(u, t, \vec{x})$ are called the Poincaré coordinates.

2.3 Thermal Field Theory

From the quantum statistics theory, we know that the finite temperature can be expressed as periodic imaginary part of time. Here we give an simple example of neutral scalar field theory [19]. Without chemical potential, the field operator in Heisenberg picture is

$$\hat{\phi}(x) = \mathrm{e}^{it\hat{H}}\hat{\phi}(0)\mathrm{e}^{-it\hat{H}}, \tag{2.23}$$

where the time coordinate $t = x^0$ is complex now. We are interesting in the thermal Green functions,

$$G_C(x_1, \cdots, x_N) = \left\langle T_C\left(\hat{\phi}(x_1)\cdots\hat{\phi}(x_N)\right)\right\rangle_\beta, \tag{2.24}$$

where the time-ordering T_C is along a complex time path C. As in the usual way, it is natural to construct the generating function $Z_C(\beta; j)$, where $j(x)$ is the source,

$$G_C(x_1, \cdots, x_N) = \frac{1}{Z(\beta)} \frac{\delta^N Z_C(\beta; j)}{i\delta j(x_1) \cdots i\delta j(x_N)}\bigg|_{j=0}.$$

One obvious solution for $Z(\beta; j)$ is

$$Z_C(\beta; j) = \mathrm{Tr}\left[\mathrm{e}^{-\beta\hat{H}} T_C \exp\left(i\int_C \mathrm{d}^4x j(x)\hat{\phi}(x)\right)\right] \tag{2.25}$$

The path C here must go through all the arguments in Green function, and $Z_C(\beta; j = 0) = Z(\beta) = \mathrm{Tr}\exp(-\beta\hat{H})$ is the partition function. Written in path integral form,

$$Z_C(\beta; j) = \int \mathcal{D}\phi \exp\left[i\int_C \mathrm{d}^4x(\mathcal{L}(x) + j(x)\phi(x))\right], \tag{2.26}$$

with a boundary condition $\phi(x^0; \mathbf{x}) = \phi(x^0 - i\beta; \mathbf{x})$.

Until now, we know the path C must start from an initial time t_i, and end at $t_i - i\beta$, meanwhile the imaginary part must be a non-increasing function. Since we are interested in Green's functions whose time arguments are real, the path should include the real axis. For simplicity, we can choose the path in the following way (figure 2.3),

1. C_1: C starts from a real time value t_i, which can be taken to negative infinity($t_i \to -\infty$), and along the real axis, C goes to $-t_i$, the positive infinity;
2. C_3: Then a jump happens, from $-t_i$ to $-t_i - i\sigma$, where $0 < \sigma < \beta$;
3. C_2: C goes leftward, from $-t_i - i\sigma$ to $t_i - i\sigma$;
4. C_4: Another jump down to $t_i - i\beta$, which is equivalent to t_i, since the time is periodic in imaginary part.

Now the free generating functional $Z_C^F(\beta; j)$ can be factorized when $t_i \to -\infty$ as

$$Z_C^F(\beta; j) = \mathcal{N} Z_{C_{12}}^F(\beta; j) Z_{C_{34}}^F(\beta; j), \tag{2.27}$$

with $C_{ab} = C_a \cup C_b$. Since $t_i \to -\infty$, $Z_{C_{34}}^F$ just gives a multiplicative constant, and we need to consider $Z_{C_{12}}^F$ only.[1]

We are not planning to give more about thermal field theory here, but the basic idea is shown above. I hope that is enough to understand the calculation of the correlation functions in AdS_5 black hole.

[1]We can see the similar structure in Schwarzschild black hole in chapter 3, and some kind of different structure in charged case in chapter 4.

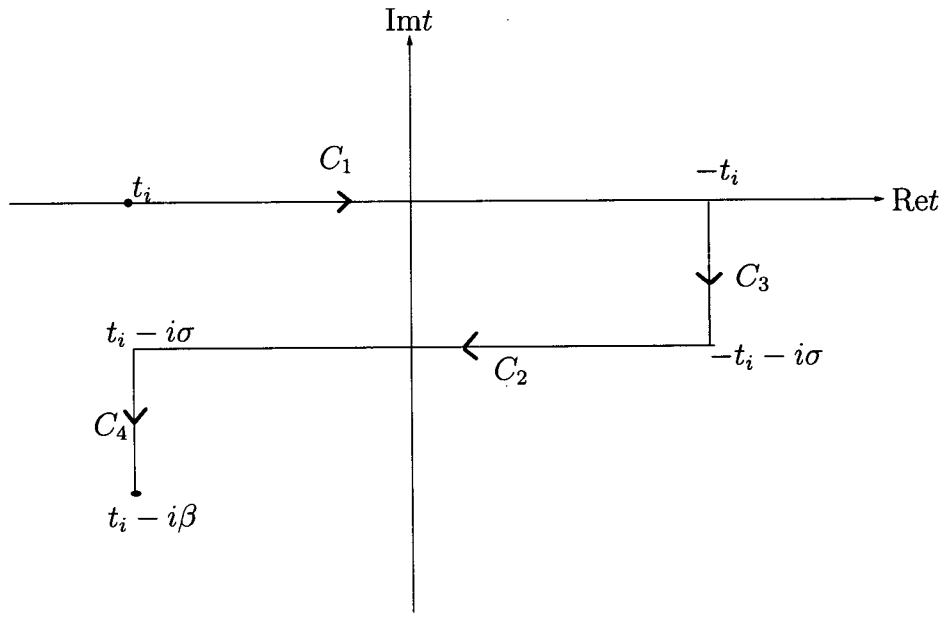

Figure 2.3: **A simple choice of time path in finite temperature β.**

2.4 AdS/CFT Correspondence

Several years ago, a conjecture was proposed that there is a connection between type IIB string theory compactified on $AdS_5 \times S^5$ and $\mathcal{N} = 4$ super-Yang-Mills theory. From then on a lot of evidence has been given.

A naive way to understand the correspondence is as following. In a 10 dimensional flat spacetime, we turn on N parallel D3 branes, then there are two different descriptions. One is from the open strings point of view, which are excitations of the D-branes. The theory is $\mathcal{N} = 4$ vector supermultiplet in (3+1) dimensions, and the low energy effective Lagrangian is $\mathcal{N} = 4$ $U(N)$ super-Yang-Mills theory. From the other side, we consider about the supergravity. When the spacetime is very closed to D3-branes, it has the structure of $AdS_5 \times S^5$. As discussed in the introduction of AdS space, there is an identical relation between the conformal boundaries of these two spaces. Naturally we will propose a conjecture that in the low energy limit, the supergravity in $AdS_5 \times S^5$ is identical with the $\mathcal{N} = 4$ $U(N)$ super-Yang-Mills theory on D3-branes, and even more, the supergravity in the whole spacetime corresponds to $\mathcal{N} = 4$ vector supermultiplet arising from D3-branes. It is generally believed that supergravity theories in different spacetime have their dual partners in different field theories. Here we restrict our discussion in the original and simplest case, $AdS_5 \times S^5$.

At first, let us start from a type IIB superstring theory in 10 dimensional flat Minkowski space. Consider N parallel D3 branes, extended along (3+1) of (9+1) spacetime coordinates, which sit together or very close to each other. There are two kinds of perturbative excitations in string theory, closed strings and open strings. The closed strings are excitations from empty space and the open ones, ended on the D-branes, are excitations of the

D-branes.

In low energy limit, when $E < 1/l_s$, we just need to consider the massless string states. The closed string massless states give a gravity supermultiplet in 10 dimensional space, with the low energy effective Lagrangian as type IIB supergravity. On the other hand, the open string massless states relate to $\mathcal{N} = 4$ vector supermultiplet in (3+1) dimensions, and the low energy effective Lagrangian is $\mathcal{N} = 4$ $U(N)$ super-Yang-Mills theory.

The complete effective action of massless modes is

$$S = S_{bulk} + S_{brane} + S_{int} \tag{2.28}$$

which just contains the massless states, integrating out all the massive fields. S_{bulk} is the action of 10 dimensional supergravity, plus some higher derivative corrections. The brane action S_{brane} is defined in (3+1) dimensions, containing the $\mathcal{N} = 4$ super-Yang-Mills Lagrangian plus some higher derivative corrections. S_{int} describes the interactions between branes modes and bulk modes.

The bulk action can be expanded as a free quadratic part describing the propagation of the free massless modes, plus some interaction terms which are proportional to positive powers of the square root of the Newton constant.

$$S_{bulk} \sim \frac{1}{2\kappa^2}\int \sqrt{g}\mathcal{R} \sim \int (\partial h)^2 + \kappa(\partial h)^2 h + \cdots, \tag{2.29}$$

where we have written the metric as $g = \eta + \kappa h$. We can do the similar expansion for S_{brane} and S_{int}. In the low energy limit, all terms proportional to κ drop out, and the gravity becomes free at long distances.

Consequently, in the low energy limit, the action decouples to two parts, one is the free supergravity in the bulk, and the other is a pure $\mathcal{N} = 4$ U(N) gauge theory in (3+1) dimensional spacetime, which is known as a conformal field theory.

Next, we consider from a different point of view. D-branes are massive charged objects, acting as sources for the various supergravity fields. The D-brane solution of supergravity can be written as

$$\begin{aligned} \mathrm{d}s^2 &= f^{-1/2}(-\mathrm{d}t^2 + \mathrm{d}x_1^2 + \mathrm{d}x_2^2 + \mathrm{d}x_3^2) + f^{1/2}(\mathrm{d}r^2 + r^2\mathrm{d}\Omega_5^2), \\ F_5 &= (1+*)\mathrm{d}t\mathrm{d}x_1\mathrm{d}x_2\mathrm{d}x_3\mathrm{d}f^{-1}, \\ f &= 1 + \frac{R^4}{r^4}, \qquad\qquad R^4 = 4\pi g_s \alpha' {}^2 N. \end{aligned} \tag{2.30}$$

Because g_{tt} is not a constant, we have

$$E = f^{-1/4}E_p, \tag{2.31}$$

where E is the energy measured by an observer at infinity, and E_p is measured by an observer at a constant radius position r. This equation can be called a red-shift relation, because when $r \to 0$, which means the object goes to the horizon, the energy E measured from an observer at infinity goes to arbitrary small, similar to an object falling into a blackhole.

So from the point of view of an observer at infinity, it is clear there are two different kinds of excitations in the low energy limit of this system, one is the free bulk supergravity, and the second is the near horizon ($r = 0$) geometry. The first one seems trivial, so we focus on the region near the horizon. For $r \to 0$, we can approximate $f \sim R^4/r^4$, so the metric now is

$$\mathrm{d}s^2 = \frac{r^2}{R^2}(-\mathrm{d}t^2 + \mathrm{d}x_1^2 + \mathrm{d}x_2^2 + \mathrm{d}x_3^2) + R^2\frac{\mathrm{d}r^2}{r^2} + R^2\mathrm{d}\Omega_5^2, \tag{2.32}$$

which is the geometry of $AdS_5 \times S^5$.

Now for the same system in the low energy limit, we have two different descriptions, both of which consist of two pieces of solutions. With a same part in both, it is natural to guess that the other part is identified with each other. So the conjecture is $\mathcal{N} = 4$ U(N) super-Yang-Mills theory in (3+1) dimensions is the same as (or dual to) type IIB superstring theory on $AdS_5 \times S^5$, which is usually called as AdS/CFT correspondence.

We check the equivalence of groups of the two theories here. For type IIB superstring theory in $AdS_5 \times S^5$, the symmetry is obviously $SO(4,2) \times SO(6)$, which gives 32 supercharges. For the $\mathcal{N} = 4$ SYM theory, on the other hand, the naive symmetry group is $SO(3,1) \times SO(6)$, where $SO(3,1)$ comes from the Lorentzian group and the symmetry of the 6 dimemsions other than (3+1) contributes to a $SO(6)$ group, giving 6 scalars. In $\mathcal{N} = 4$ supersymmetry, the fermions can be shown as ψ^a, (a=1,...,4), and there are 16 supercharges. After adding the dilaton and special conformal transformation symmetry, the group is extended to $SO(4,2)$, with another series of fermions, λ^a, and the total supercharges now is 32, the same as in $AdS_5 \times S^5$ case. In a word, both the theories have the same supergroup.

It is helpful to show some properties in understanding the correspondence of the AdS/CFT.

Field $\leftrightarrow$ operator correspodence

In conformal field theory, there is no asymptotic states or S-matrix, so we need to consider just operators. For example, in $\mathcal{N} = 4$ super-Yang-Mills theory, give a deformation by a marginal operator, which will change the coupling constant of the gauge theory. Since $\mathcal{N} = 4$ super-Yang-Mills theory is one part of the low energy limit of the string theory, changing the gauge coupling constant relates to changing of the coupling constant in string theory, which is also the expectation value of the dilaton. Such a dilaton expectation value is determined by the boundary condition for the dilaton at infinity. More precisely, we put in a operator $\mathcal{O}$ in conformal field theory, so a term $\int \mathrm{d}^4x\phi_0(\vec{x})\mathcal{O}(\vec{x})$ can be added in the Lagrangian. On the AdS side, we can change the boundary condition of dilaton at the boundary, $\phi(\vec{x}, z)|_{z=0} = \phi_0(\vec{x})$. The correlation is

$$\left\langle e^{\int \mathrm{d}^4x\phi_0(\vec{x})\mathcal{O}(\vec{x})} \right\rangle_{CFT} = Z_{string}\left[\phi(\vec{x}, z)|_{z=0} = \phi_0(\vec{x})\right]. \tag{2.33}$$

where the left side is the generating function of correlation functions in field theory, that is, ϕ_0 is an arbitrary function and we can calculate the correlation functions of $\mathcal{O}$ by taking functional derivatives and set ϕ_0 to zero. The right side is the full partition function of

string theory with boundary condition $\phi = \phi_0$ on the boundary of AdS. Therefore each field propagating on AdS generally one-to-one corresponds with an operator in the field theory. And there is a relation between the mass of the field ϕ and the scaling dimension of the operator $\mathcal{O}$ in CFT.

Holography

Here we will show that the AdS/CFT correspondence gives a holographic description of the physics in AdS space.

One of the most famous holography is the Bekenstein bound, which states that the maximal entropy of a volume is $S_{max} = Area/4G_N$, where the area is the volume of the one less dimension boundary surface. Such a relation is usually called as "holography principle", which is connected with the second law of thermal dynamic. Another expression of the principle in quantum gravity is that all physics within some volume can be described in terms of some theory on the boundary which has less than one degree of freedom per Planck area.

In our case, the AdS/CFT correspondence states that the physics in AdS space can be described by a field theory in one less dimensional space, which is a natural holography. However it is difficult to compare the number of degrees of freedom, because the conformal theory has infinite degree of freedom, as well as the boundary area of AdS space. So we try to introduce a cut-off here. Rewrite the metric of AdS,

$$\mathrm{d}s^2 = R^2 \left[-\left(\frac{1+r^2}{1-r^2}\right)^2 \mathrm{d}t^2 + \frac{4}{(1-r^2)^2}(\mathrm{d}r^2 + r^2 \mathrm{d}\Omega^2) \right], \tag{2.34}$$

here the boundary of AdS is at $r = 1$. We see that in conformal group on Poincaré coordinates, radial position has a role of energy scale in field theory, since when we approach the boundary we do a conformal transformation which localizes the objects in CFT. So we can specify the boundary position at $r = 1 - \delta$. The limit $\delta \to 0$ corresponds to the UV region of the field theory, and setting δ to a small number relates to a UV cut-off. Such a relation is also called a UV-IR relation.

Consider a $\mathcal{N} = 4$ super-Yang-Mills theory on S^3 with radius 1, if we set a UV cut-off δ, the degree of freedom is

$$S \sim N^2 \delta^{-3}. \tag{2.35}$$

On the other hand, in gravity solution, the area in Planck units of the surface $r = 1 - \delta$,

$$\frac{Area}{4G_N} \sim N^2 \delta^{-3}, \tag{2.36}$$

which is exactly the same as before. So we see that the AdS/CFT correspondence saturates the holographic bound.

However it is incorrect to think that AdS/CFT correspondence means that at the same time an additional field theory lives at the boundary. Different regions of AdS, with different radial positions, correspond to different energy scales in the field theory. So the "boundary" we say here has not the usual meaning, more close to a one less dimension

sense. It is helpful and interesting to consider different boundaries, which give us different AdS structures. In Poincaré coordinates, the boundary is $\mathbf{R}^{3+1}$. Since the space is infinity, there is no mass gap, and the excitations can be with arbitrarily low energy, which means a horizon since when an object falling to it the energy measured from infinity is arbitrarily small. In global coordinates, we have a boundary of $S^3 \times \mathbf{R}$, so, different from the first case, we have a mass gap, a horizon, and a discrete spectrum.

Correlation functions

In the low energy limit, we can approximate the string partition function as $e^{-I_{SUGRA}}$, where I_{SUGRA} is the supergravity action in $AdS_5 \times S^5$. In this approximation we ignore all the stringy α' corrections and loop corrections, and in the gauge field theory language, it means to take large N and $g_{YM}^2 N$ limit. The basic relation is

$$e^{-I_{SUGRA}} \simeq Z_{string} = Z_{gauge} = e^{-W}, \tag{2.37}$$

where W is the generating functional for connected Green's functions in the gauge theory. At finite temperature, we can write $W = \beta F$, where β is the inverse temperature and F is the free energy of the gauge theory. Apply this relation to a Schwarzschild black hole, it is thought in gauge theory a thermal state at temperature T, which is the Hawking temperature of the black hole.

We turn on a boundary condition $\phi(\vec{x}, z)|_{z=\epsilon} = \phi_0$, which play a role of source for gauge-invariant operators in the field theory. Extremizing the action $I_{SUGRA}[\phi]$ to saddle points with the boundary condition gives us the equations of motion in the bulk. So we can write

$$W_{gauge}[\phi_0] = -\log \left\langle e^{\int \mathrm{d}^4 x \phi_0(x) \mathcal{O}(x)} \right\rangle_{CFT} \simeq \underset{\phi|_{z=\epsilon} = \phi_0}{\text{extremum}} \; I_{SUGRA}[\phi] \tag{2.38}$$

That is, the generator of the connected Green's functions in the gauge field theory, in the large N, $g_{YM}^2 N$ limit, is the on-shell supergravity action.

Thermal phase transition

When we extremize an action, sometime there are more than one saddle points, which compete to minimize it and to dominate the correlation functions, so there can be phase transition points between them. At such transitions, the saddle points exchange their domination.

Consider the supergravity action in AdS_5,

$$I = -\frac{1}{16\pi G_5} \int \mathrm{d}^5 x \sqrt{g} \left(\mathcal{R} + \frac{12}{R^2} \right), \tag{2.39}$$

where $\mathcal{R}$ is the Ricci scalar and R is the radius of anti-de Sitter space. we have two different solutions, a Schwarzschild black hole in AdS space, and a thermal gas of particles in AdS space.

At finite temperature T, we consider a field theory on S^3, now turn on the Euclidean time, which is periodic with $t \sim t+\beta$, where $\beta \sim 1/T$. As discussed before, the boundary of AdS_5 now is $S^3 \times S^1$. However the two solutions relate to different bulk structures. For the black hole in AdS the bulk is $S^3 \times B^2$, or we can indicated as X_2. For the thermal gas case, the system has a bulk structure of $B^4 \times S^1$, called X_1. Now the S^1 is not simply connected, so there are two possible spin structures on X_1, corresponding to thermal(anti-periodic) or supersymmetric(periodic) boundary conditions on fermions. In contrast, X_2 is simply connected, so there is just one spin structure, corresponding to thermal boundary conditions. So in computing for twisted partition functions, $\mathrm{Tr}(-1)^F e^{-\beta H}$, just X_1 contributes; while for usual thermal partition functions, Tr $e^{-\beta H}$, we need to consider both X_1 and X_2, with the important one dominating. Because $I(X_1)$ and $I(X_2)$ are both infinite, we consider

$$I(X_2) - I(X_1) = \frac{\pi^2 r_+^3 (R^2 - r_+^2)}{4G_5(2r_+^2 + R^2)}. \tag{2.40}$$

Obviously there is a transition when $R = r_+$.

Such a transition is a confinement-deconfinement transition. Deconfinement at high temperature can be characterized by a spontaneous breaking of the center of gauge group. In our $SU(N)$ group, the center is $\mathbb{Z}_N$. The order parameter of the breaking of the center is the expectation value of Polyakov (temporal) loop $\langle W(C)\rangle$, where C, in our case, is a path around S^1, in the common boundary $S^3 \times S^1$ of X_1 and X_2. With a element $g \in \mathbb{Z}_N$ acted, the $\langle W(C)\rangle \to g\langle W(C)\rangle$. The expectation value of Polyakov loop measures the change of the free energy of the system $F_q(T)$ induced by an external charge q, $\langle W(C)\rangle \sim \exp(-F_q(T)/T)$. In a confining phase $F_q(T)$ is infinite and so $\langle W(C)\rangle = 0$, while in a deconfining system $F_q(T)$ is finite and so $\langle W(C)\rangle \neq 0$.

So it is clear that at low temperature, our bulk has a structure of X_1. A contour C wraps on S^1 is not a boundary of any 2 dimensional manifold D, which implies that $\langle W(C)\rangle = 0$, and the system is confined. At high temperature, we have X_2 as the bulk structure, and now C is a boundary of a string worldsheet $D = B^2$, so $\langle W(C)\rangle \neq 0$ and the system is in a deconfined phase.

To be more clear, we outline the correspondence here again. At low energy limit, in which $\alpha' \to 0$ and $\lambda = g_{YM}^2 N \to +\infty$, a type IIB supergravity has two solutions, AdS space and a Schwarzschild black hole in AdS space. AdS dominates at low temperature while the other is more important at high temperature, so there must be a transition at some temperature. On the other hand, when $\lambda = g_{YM}^2 N \to 0$, the $\mathcal{N} = 4$ super-Yang-Mills theory contains two different solutions, one is a confined state which is more significant at low temperature, and the other one is a deconfined state dominating at high temperature. Also there is a transition between them. It is natural to guess that there is a relation between these two transitions of different languages of the "same" system. However notice that they are valid at different limits, $\alpha' \to 0 (\lambda \to \infty)$ and $\lambda \to 0$, the AdS/CFT correspondence is not so clear. But we have many examples to show that this is a pretty good duality. Another remarkable work is [20]. In a pp wave background, we can calculate the exact string solutions, which show that for any α', a transition described as before exists. So in this way, can we get the same description as in type IIB supergravity when $\alpha' \to 0$? If we can, we prove the AdS/CFT correspondence in more sense.

Chapter 3

AdS Schwarzschild black hole

In an *AdS* Schwarzschild black hole of $d \geq 3$ dimensions, there are two parameters, in which one is the mass and the other is the *AdS* radius. For simplicity, we will focus on the large black hole limit, where the *AdS* radius is much smaller than the horizon radius. Here we consider mostly in $d = 5$ case, comparing with $d = 3$ BTZ black hole.

The metric of 5-dimensional *AdS* Schwarzschild black hole is given by

$$\begin{aligned} \mathrm{d}s^2 &= -f(r)\mathrm{d}t^2 + \frac{\mathrm{d}r^2}{f(r)} + r^2\mathrm{d}\Omega_3^2, \\ f(r) &= \frac{r^2}{l^2} + 1 - \frac{r_+^2}{r^2}(\frac{r_+^2}{l^2} + 1) \end{aligned} \tag{3.1}$$

where r_+ is the horizon radius and l is the *AdS* radius. In the infinitely massive limit $r_+/l \to \infty$, the metric is much simplified. And if we rescale the coordinates $r \to \frac{r_+}{l}r$, $t \to \frac{l}{r_+}t$, and set $l = 1$, also we neglect the angular part, the metric becomes

$$\begin{aligned} \mathrm{d}s^2 &= -f(r)\mathrm{d}r^2 + \frac{\mathrm{d}r^2}{f(r)}, \\ f(r) &= r^2 - \frac{1}{r^2} \end{aligned} \tag{3.2}$$

Obviously the genuine curvature singularity is at $r = 0$, and the boundary of the spacetime is approached at the horizon $r = 1$. Also there is a coordinate singularity at the horizon $r = 1$, for which we can transfer to Kruskal coordinates (T,X) to remove the singularity. However it is more convenient to discuss the global extension with complexified time,

$$t = t_L + it_E, \tag{3.3}$$

where t_L and t_E denote the times on Lorentzian and Euclidean slices separately. The whole spacetime contains four coordinate patches (two asymptotic (boundary) regions (I and III) with $r > 1$, the regions inside the black hole (II) and the white hole (IV) with $r < 1$). In each patch, time has a constant imaginary part and the real part goes to $\pm\infty$ when $r = 1$, which are the boundaries of the patches. The Euclidean time $t = it_E$ is a periodic imaginary one, with period of β, the inverse of temperature T of the black hole. We define $t_E = 0$ in the region I, and the t_E of the other patches are shown in figure 3.1. Crossing a horizon shifts t_E by $i\beta/4$. In the geometry (3.2), $\beta = \pi$.

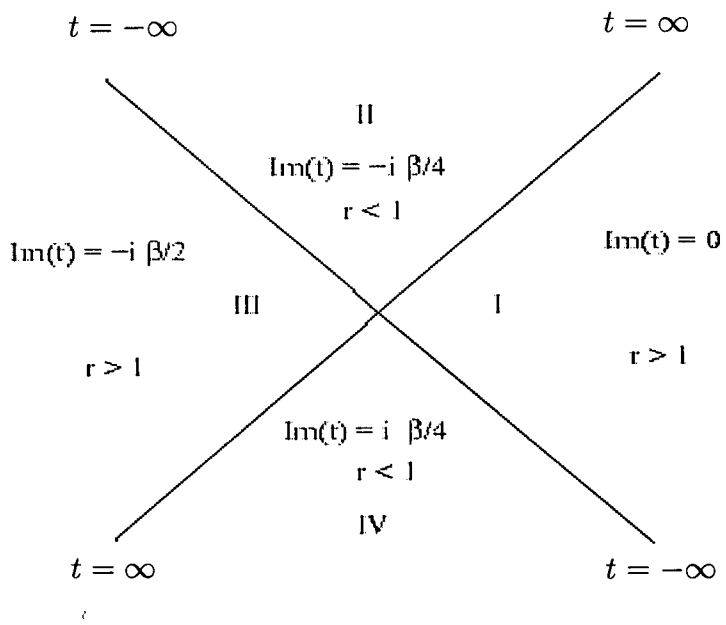

Figure 3.1: **Complexified coordinates for *AdS* Schwarzschild black hole**: the time coordinate is complex, with a constant imaginary part in each wedge, The wedges are separated by horizons $r = 1$ (the 45 degree lines in the diagram), which relate to $t_L = +\infty$ or $t_L = -\infty$.

3.1 Radial null geodesics

We now consider the geodesics, which can give the global spacetime structure and the correlators. Radial geodesics $x = (t(s), r(s))$ (s is an affine parameter) can be found by extremizing the action

$$S = \int \mathrm{d}s \, g_{\mu\nu} \dot{x}^\mu \dot{x}^\nu, \tag{3.4}$$

where $\dot{x} = \frac{\mathrm{d}x}{\mathrm{d}s}$. Requiring $\dot{x}^2 = 0, +1, -1$ is for null, spacelike, and timelike geodesics respectively.

For the null geodesics, the equations are

$$\dot{t} = \frac{E}{f(r)}, \qquad \dot{r}^2 = E^2. \tag{3.5}$$

Along a geodesic starting from the boundary at $t = t_0$, the time is

$$t(r) = \int \frac{\dot{t}}{\dot{r}} \mathrm{d}r' = t_0 + \int_r^\infty \frac{\mathrm{d}r'}{f(r')} \tag{3.6}$$

For $r < 1$,

$$t(r) = t_0 - \frac{1}{2}\left[\tan^{-1} r - \frac{\pi}{2} - \tanh^{-1} r\right] - i\frac{\pi}{4}. \tag{3.7}$$

When $t_0 = 0$, $t(0) = \pi/4(1 - i)$, which means that a null geodesic starting from the boundary at $t_0 = 0$ gets the singularity $r = 0$ at a time with positive real part. As shown in figure 3.2 the boundaries and the singularities cannot be both straight in its Penrose diagram. If we make the boundaries straight, the singularities should be bowed in, or with straight singularities, the boundaries must be bowed out. Conversely, for a null geodesic reaching the center of singularity ($t = 0$, $r = 0$), it must start from the boundary at

$$t_c = -\pi/4 = -\beta/4. \tag{3.8}$$

In general dimension d, $t_c = -\pi \left((d-1)\tan\frac{\pi}{(d-1)}\right)^{-1}$, which vanishes only for $d = 3$. Thus different from $d = 3$ BTZ black hole, all the $d > 3$ singularities are bowed as in figure 3.2b.

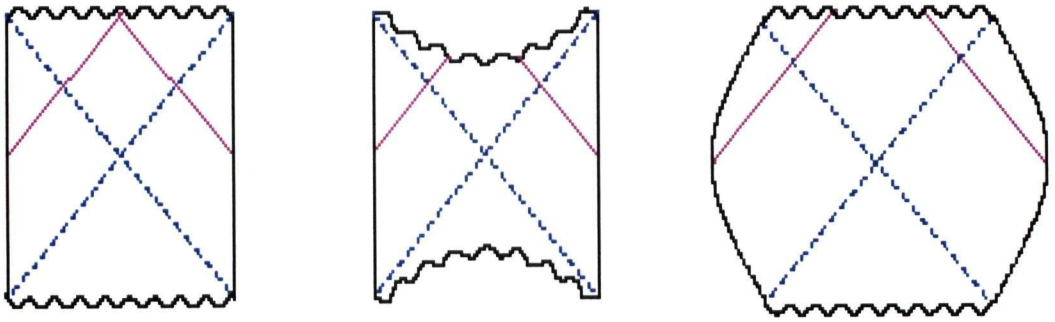

Figure 3.2: **Penrose diagrams**: the solid lines of both sides are boundaries, the wavy lines are spacelike singularity $r = 0$, the dashed 45 degree lines are the horizons, and the solid 45 degree lines are null radial geodesics. If the geodesics meet at singularity, the diagram can be drawn as a square (a); if they don't, (b) can be conformally transformed to (c). From above, behavior of null radial geodesics can give the shape of Penrose diagram.

We can get the same result by investigating the Kruskal coordinates (T,X), as illustrated in figure 3.3, where the future and past singularities are the hyperbolas $T^2 - X^2 = 1$. In $d = 3$ BTZ black hole, the boundaries are at $T^2 - X^2 = -1$, while the AdS boundaries are at $T^2 - X^2 = -\pi/2$ in $d = 5$ AdS black hole.

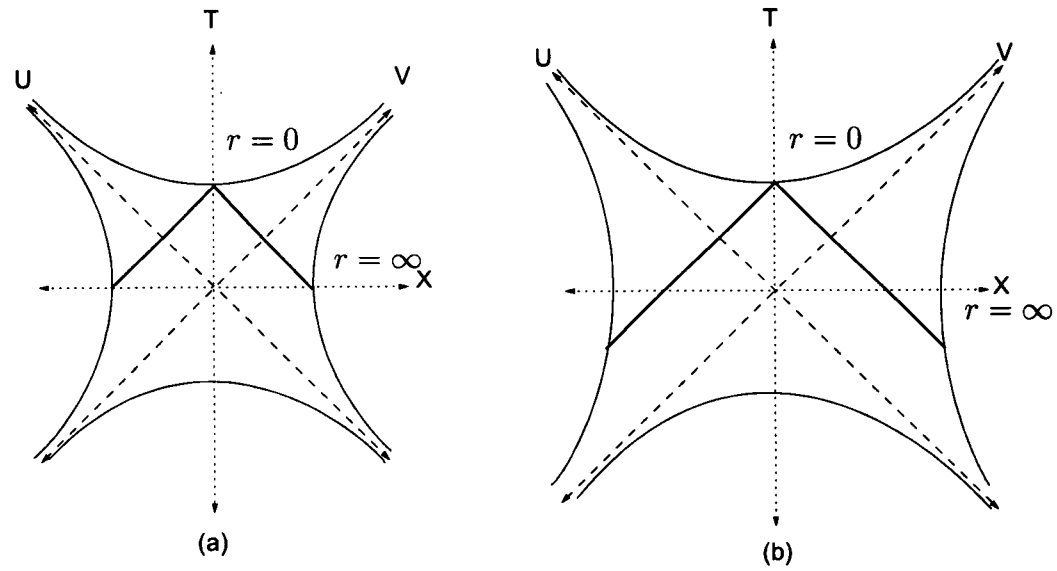

Figure 3.3: **Radial null geodesics on Kruskal diagrams**, a) for $d = 3$, BTZ black hole; b) for $d > 3$, *AdS* black hole. For two geodesics meeting at the center of singularity, they start from boundaries at a) $t = 0$; b) $t = -t_c < 0$.

3.2 Radial spacelike geodesics

Focusing on the correlator of two points at different boundaries, we need to consider the spacelike geodesics connecting them. The spacelike geodesics satisfy $\dot{x}^2 = -f(r)\dot{t}^2 + \frac{\dot{r}^2}{f(r)} = 1$, giving

$$\dot{t} = \frac{E}{f(r)}, \qquad \dot{r}^2 - f(r) = E^2. \tag{3.9}$$

Here E is a conserved quantity from time translation symmetry, or we say energy. This equation is just similar to a particle with energy E^2 moving in a potential $V(r) = -f(r)$. When E is zero, the minimal radius a particle can get is just the horizon r_+, and with the E^2 increase the particle can reach behind the horizon and more and more close to singularity $r = 0$. However, from the figure 3.4 we know that in a $d = 5$ Schwarzschild black hole, a particle with any finite energy can never reach the singularity, which means in geometry language, a spacelike geodesic always connects two boundary points. In Penrose diagram, the 45 degree line are null geodesics, so a spacelike one is with a more gentle slope everywhere. So it is easy to see that the two boundary points connected by a spacelike geodesic are at different sides. In the corresponding conformal gauge field theory of the asymptotic boundaries, that is just a correlator between them.

We plot some symmetric geodesics in figure 3.5. When $E = 0$, it is the center horizontal line, connecting the two $t = 0$ points of the boundaries. When E^2 goes to infinity, the geodesics seems almost null and hit the "middle" of singularities at the limit. Such a geodesic starts from the boundaries at time $|t| = t_c$. Out of this region there is no symmetric

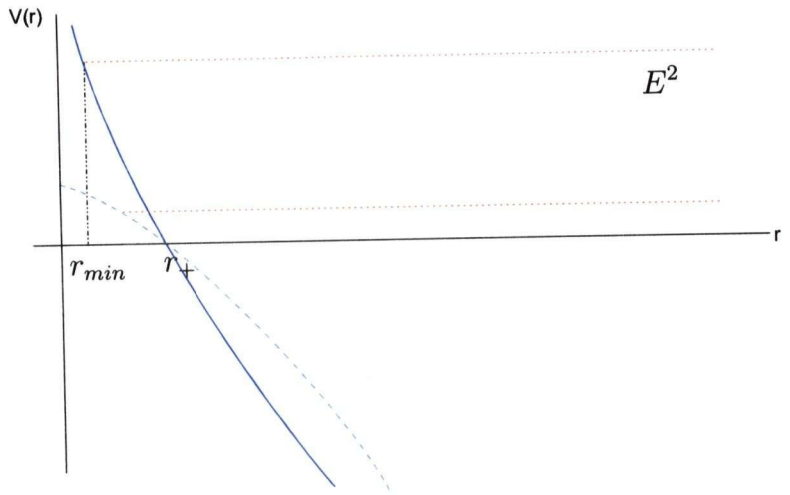

Figure 3.4: **The potential** $V(r) = -f(r)$: the dashed cyan line is for $d = 3$ BTZ black hole, and the solid blue line is for $d = 5$ Schwarzschild case. With a great enough conserved energy E^2, a particle can approach the $r = 0$ singularity in BTZ case, but in $d = 5$ dimension, it will always be bounced back at some radius $0 < r_{min} < r_+$ to the boundary.

spacelike geodesic.

Let us consider the $E = 0$ case first. Starting from the center of right side boundary $t = 0$, the geodesic reach the horizon $r = r_+ = 1$ and is bounced "back" to another boundary, keep $t_L = 0$ everywhere. The proper length along such a geodesic is

$$\mathcal{L} = 2\int_1^{r_{max}} \frac{\mathrm{d}r}{\dot{r}} = 2\int_1^{r_{max}} \frac{\mathrm{d}r}{\sqrt{f(r)}}, \tag{3.10}$$

where r_{max} is the radius of boundaries. Integrating out the result

$$\mathcal{L} = \ln\left(r_{max}^2 + \sqrt{r_{max}^4 - 1}\right) \approx 2\ln r_{max} + \ln 2 + \mathcal{O}(r_{max}^{-4}). \tag{3.11}$$

When $r_{max} \to \infty$, the proper length is logarithmically divergent, and we can regularize it as

$$\mathcal{L}_{reg} = \ln 2. \tag{3.12}$$

Turning on the energy now, a symmetric geodesic leave the center at the boundary. From the spacelike geodesic equations (3.9), we know that at the turning point

$$E^2 + f(r_i) = 0. \tag{3.13}$$

So $r_i < 1$, just as the curved geodesics shown in figure 3.5. For such a geodesic, the turning point $r = r_i$ must be in region II with $t_E(r_i) = -\beta/4$, and $t_L(r_i) = 0$ required by symmetric

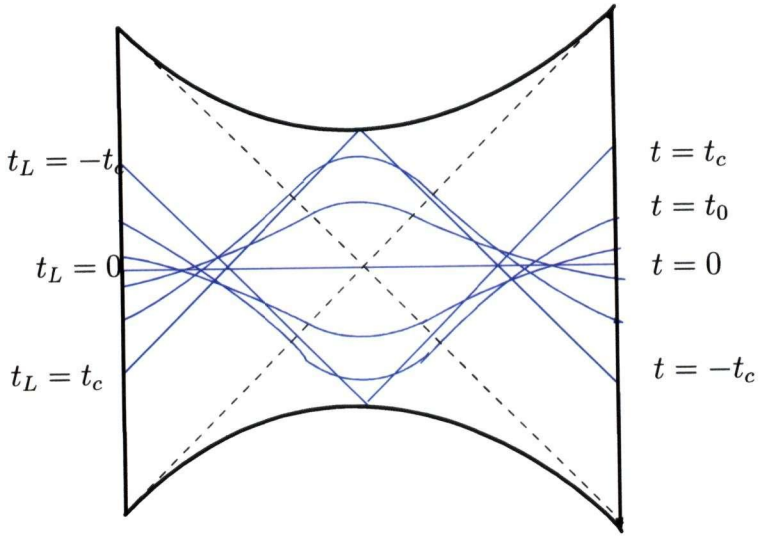

Figure 3.5: **Some symmetric spacelike geodesics in the Penrose diagram.** The geodesics are shown as blue lines. In the Penrose diagram, we draw the boundaries straight, so the future and past singularity must be bowed in. The dashed 45 degree lines are the horizons $r = r_+$. When E^2 goes to infinity, the spacelike geodesics, starting from the boundaries at $t = t_c$, are almost null and very closed to singularity. Out of the region there is no such symmetric spacelike geodesic.

condition. The geodesic equation gives the starting boundary time t_0,

$$t_0 - t(r_i) = t_0 + i\beta/4 = -\int_{r_i}^{\infty} \frac{\dot{t}}{\dot{r}} \mathrm{d}r = -\int_{r_i}^{\infty} \frac{E}{f(r)\sqrt{E^2 + f(r)}} \mathrm{d}r. \tag{3.14}$$

Easy to check that when $E = 0$, $t_0 = 0$, and also $t_0 \to t_c$ as $E \to \infty$.

The proper length with energy E is

$$\mathcal{L} = 2\int_{r_i}^{r_{max}} \frac{\mathrm{d}r}{\sqrt{E^2 + f(r)}}. \tag{3.15}$$

Up to regularization,

$$\mathcal{L} = \ln\left(\frac{2}{\sqrt{E^4/4 + 1}}\right). \tag{3.16}$$

When $E = 0$, the equation (3.12) is recovered. On the other hand, in the $E \to \infty$ limit, the geodesics go to the null geodesics bounced off the singularity, and the proper length

$$\mathcal{L} \sim 2\ln(t - t_c). \tag{3.17}$$

There is a singularity at the limit $t \to t_c$ ($E \to \infty$).

3.3 Correlation functions

According to the AdS/CFT correspondence, AdS Schwarzschild black hole in $d = 5$ is dual to $\mathcal{N} = 4$ SYM theory at finite temperature. In the large black hole limit, the CFT is effectively in an infinite volume. The standard CFT correlator at finite temperature is dual to bulk correlation with insertions in the same asymptotic region, say region I. Also we can define other kinds of correlators, such as putting two operators on different boundaries, of region I and region III.

In the real-time formalism, we have two copies of original field theories. The total Hamiltonian can be written as

$$H_t \equiv H \otimes I - I \otimes H^*, \tag{3.18}$$

where H is the Hamiltonian for the original theory and H^* is for the field theory on the other boundary. And the entangled state is

$$|\psi\rangle = \frac{1}{Z^{1/2}} \sum e^{-\frac{1}{2}\beta E_i} |E_i, E_i\rangle, \tag{3.19}$$

where $|E_i, E_j\rangle = |E_i\rangle \otimes |E_j\rangle$, $|E_i\rangle$, $|E_j\rangle$ are the eigenstates.

We use 1, 2 to label the two subsystems. An operator of subsystem 1 has the form $A_1 \equiv A \otimes I$, and $A_2 \equiv I \otimes A^\dagger$ for subsystem 2. The correlation function defined in the subsystem 1 is

$$\langle\psi|A_1(0)B_1(t)|\psi\rangle. \tag{3.20}$$

If we consider an operator A_1 in subsystem 1 and B_2 in subsystem 2, the correlator is now

$$\langle\psi|A_1(0)B_2(t)|\psi\rangle. \tag{3.21}$$

We can check by analytically continuing that

$$\langle\psi|A_1(0)B_2(t)|\psi\rangle = \langle\psi|A_1(0)B_1(-t - i\beta/2)|\psi\rangle. \tag{3.22}$$

So a two sided correlator is just as an ordinary thermal correlator.

Now we assume there is a scalar field with mass m, propagating in the bulk. So a 2-point correlation function is determined by the bulk propagator, which is the sum of all paths between these 2 points, with each as $e^{-m\mathcal{L}}$, $\mathcal{L}$ is the proper length of the path. In the large mass m limit, the propagator, as well as the correlator, is dominated by the shortest path, which is dual to the shortest geodesic between the 2 points in AdS space.

t_c singularity and complex geodesics

From equation (3.17), the proper length has a logarithmical divergence around $t = t_c$, so the correlation function is

$$e^{-m\mathcal{L}} \sim \frac{1}{(t - t_c)^{2m}}. \tag{3.23}$$

We have a singularity when the spacelike geodesic goes to almost null.

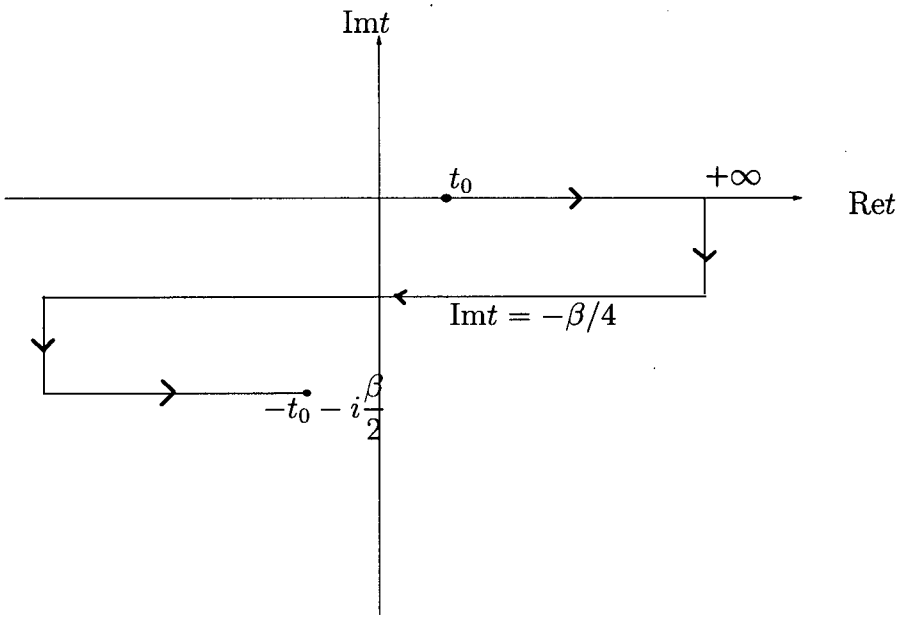

Figure 3.6: **The path of time in Schwarzschild case in path integral of a two-point correlation function, which ends at the boundaries of different sides.**

However we can show that

$$|\langle\phi_2(t)\phi_1(-t)\rangle_\beta| \leq \langle\phi_2(0)\phi_1(0)\rangle_\beta \tag{3.24}$$

for any Hermitian operator ϕ. And the $\langle\phi_2(0)\phi_1(0)\rangle_\beta$ can be calculated as a finite value. Therefore we have a puzzle between the naive t_c singularity and the analysis from field theory.

With a close investigation, we find that around $E = 0$

$$\begin{aligned} t &\sim E^3, \\ \mathcal{L} &\sim -E^4, \\ \mathcal{L} &\sim -t^{4/3}. \end{aligned} \tag{3.25}$$

So there is a branch point at $t = 0$. In the 3 branches, two of them are complex. It is easy to check that the two complex branches are more important than the real one around $t \sim 0$. We can analytically continue to general E region. Complex values of E correspond to goedesics in the comlixified AdS Schwarzschild spacetime, where both r and t are complex. Therefore the correlator in gauge theory must become complex after a certain time. When $t \to t_c$, the correlator is still dominated by the two complex geodesics, which give the same contribution, with the t_c singularity given by the subdominated real geodesic. The complex branches have no t_c singularity, and that explains its absence in gauge theory.

Fortunately, we need not consider such complex branches in charged black hole case,

where

$$\mathcal{L} \sim t^2, \tag{3.26}$$

when $E \longrightarrow 0$, which is different from equation (3.25).

Chapter 4

Charged Black Hole in AdS space

[1] We have reviewed the analysis in AdS Schwarzschild black hole, with the calculation of proper length of spacelike geodesics between different boundary spacetime, and also the corresponded correlation functions in gauge theory, from which we can reach the region behind the horizon. In this chapter, we extend to charged AdS_5 black hole in a similar way. However, we found many significant differences from Schwarzschild case.

In section 4.1, we analyze the classical geometry of the AdS_5 charged black hole. From the metric, we give the spacetime structure and the Penrose diagram, which shows that the imaginary part of time is periodic in a complicated way, and the regions with different constant imaginary time are separated by event and Cauchy horizons. We also give the Kruskal coordinate system, which makes the causal structure very clear.

Then in section 4.2, we make some discussion about neutral correlation functions. With a probe neutral particle, we consider the spacelike geodesics without angular momentum L, ended at different sides of boundary. In addition, we have a bit of discussion of rotating spacelike geodesics. Considering the symmetric $L = 0$ spacelike geodesics, different values of energy E correspond to different boundary time $t(E)$. And with different set of parameters of the charged black hole, eg. mass and charge, the boundary time shows quite different behavior. The behavior of proper length is similar, which determines the correlation functions. Since a puzzle appears in Schwarzschild case, which makes some superficial discrepancy between the classical geometrical analysis and the gauge theory, we need to do similar thing in our case. Fortunately we find there is no such problem in charged black hole in general.

Now we turn on the charge of the probe particle. In section 4.3, we give some general discussion, comparing with the neutral probe particle.

It is well known that generally the inner horizons (Cauchy horizons) of a charged black hole are unstable with perturbation of spacetime [14, 25]. Some work investigated black holes with null perturbations which are purely ingoing, purely outgoing, or both. A phenomenon of mass inflation appears, and the spacetime effectively break down at the Cauchy horizons [21, 22, 23, 24]. In section 4.4 we turn on a null outgoing perturbation. The Cauchy horizons and inner horizons are moved and separated in some region. Meanwhile the perturbation give correction to the geodesics, which makes changes of their correspondent boundary times and proper lengths. By tuning the time t_p, when the perturbation leave the left-hand boundary, one can make a scanning (at least some of) the region between the event horizons and Cauchy horizons. One natural result is in any we can never reach the region behind the Cauchy horizon.

[1] A version of this chapter has been accepted for publication. Dominic Brecher, Jianyang He and Moshe Rozali, "On Charged Black Hole in Anti-de Sitter Space," to be appeared in JHEP [arXiv:hep-th/0410214]

4.1 Classical Geometry

In this section we discuss the classical geometry of the electrically charged AdS-RN black hole, its complexification and causal structure. We restrict attention to aspects of the geometry which are relevant for us, more details can be found in [27].

The Spacetime

The five dimensional solution of a charged black hole[2] takes the form [27]

$$ds^2 = -f(r)dt^2 + \frac{dr^2}{f(r)} + r^2 d\Omega_3^2, \qquad A = \left(-\frac{1}{c}\frac{Q}{r^2} + \Phi\right) dt \tag{4.1}$$

where

$$f(r) = 1 + \frac{r^2}{l^2} - \frac{M}{r^2} + \frac{Q^2}{r^4} \equiv \frac{\Delta(r)}{l^2 r^4}, \qquad \Delta(r) = r^6 + l^2 r^4 - l^2 M r^2 + l^2 Q^2, \tag{4.2}$$

$c = 2/\sqrt{3}$, Φ is a constant and M and Q are respectively proportional to the mass and charge of the black hole. The spacetime is asymptotically AdS, with curvature radius l, the boundary theory living on $\mathbb{R} \times S^3$. From now on, we will take $l = 1$. The boundary is at $r = \infty$ and there is a timelike singularity at $r = 0$.

We get a naked singularity if there are no real positive roots. We can derive a bound to ensure the absence of naked singularities by considering the positive extremum of $P(x)$, which occurs for $x_0 = l^2(-1 + \sqrt{1 + 3R^2/l^2})/3$. If $P(x_0) \leq 0$ we are guaranteed to have at least one positive root. This holds if

$$\left(1 + \frac{3R^2}{l^2}\right)^3 \geq \left(1 + \frac{9R^2}{2l^2} + \frac{27Q^2}{2l^4}\right)^2 \tag{4.3}$$

The extreme case, when this bound is saturated, is not supersymmetric [27]. Rather, the supersymmetric solution has a naked singularity.[3]

Horizons of the metric are given by the real positive roots of $\Delta(r)$. We will often work with the variable $x = r^2$, $\Delta(x)$ being a cubic in x. Since, with $M > 0$,

$$\Delta(0) = Q^2 > 0 \qquad \text{and} \qquad \frac{d\Delta}{dx}(0) = -M < 0, \tag{4.4}$$

one root of Δ must occur for $x < 0$. We denote this negative root by $-x_0 = -r_0^2$. There are then at most two positive real roots, denoted by $x_\pm = r_\pm^2$, with $x_+ \geq x_-$. We will thus write

$$\Delta(x) = (x + x_0)(x - x_-)(x - x_+). \tag{4.5}$$

[2] A solution of five dimensional Einstein-Maxwell theory with a negative cosmological constant. The ten dimensional origins are discussed in [27].

[3] The ten-dimensional origin of the black holes are rotating D-branes, from which the naked singularity is inherited.

It is easy to show that $x_0 = 1 + x_- + x_+$, so we will only need to specify $x_\pm$. The non-extreme black hole, with $x_+ > x_-$, has an outer event horizon at r_+ and an inner Cauchy horizon at r_-. The extreme solution, with $x_+ = x_-$, has a single event horizon at r_+.

The surface gravities at the outer and inner horizons are, respectively,

$$\kappa_\pm = \pm\frac{1}{2}\frac{\mathrm{d}f}{\mathrm{d}r}\bigg|_{r=r_\pm} = \frac{(x_0 + x_\pm)(x_+ - x_-)}{x_\pm^{3/2}}, \tag{4.6}$$

In the usual way, to avoid a conical singularity at $r = r_+$, we demand periodicity of the Euclidean time coordinate:

$$\tau \equiv \tau + \beta = \tau + \frac{2\pi}{\kappa_+}, \tag{4.7}$$

giving the black hole temperature $T = 1/\beta = \kappa_+/(2\pi)$. Note that the extreme holes have $T = 0$. The dual field theory is thus in a thermal state at temperature T. One can then work [27] with either fixed charge (the canonical ensemble) or fixed potential (the grand canonical ensemble). In the latter case, the electrostatic potential in the field theory is given by the constant Φ, which can be fixed as $\Phi = (1/c)(Q/x_+)$ such that $A_t(r_+) = 0$. In terms of the bulk physics, Φ is the electrostatic potential difference between the horizon and infinity.

Embedding into the Complex Plane

There are six distinct kinds of regions of the spacetime, the Penrose diagram consisting of an infinite sequence of these basic blocks. As was emphasized in [15], and as will be discussed below, the region behind the inner horizon does not seem to play any role in the field theory, therefore we can restrict attention to one copy of these basic blocks.

To describe the global structure, one can pass to Kruskal-like coordinates to describe the maximal analytic extension of the space. Alternatively, as in [9, 13, 14, 15], one can use different Schwarzschild coordinate patches to describe the global extension. They are embedded into complex Schwarzschild time, with $t = t_L + it_E$ having a constant imaginary part in each patch. This is shown in figure 4.1, in which we define $t_E = 0$ in the right asymptotic region. Then, as in [9], crossing the event horizon at r_+ shifts t_E by $\pi/(2\kappa_+) = i\beta/4$ so, to move from a point on the right-hand boundary to the symmetric point on the left-hand boundary, we shift $t \to -(t + i\beta/2)$. Crossing the Cauchy horizon at r_- instead would shift t_E by $\pi/(2\kappa_-)$ although this will not be relevant to the boundary field theory[4].

The Penrose Diagram

The basic features of the Penrose diagram are shown by the behaviour of radial null geodesics. As in the uncharged case [9], the boundaries and the singularities cannot both be drawn as straight lines. For radial null geodesics, we work with the Lagrangian

$$\mathcal{L} = -f(r)\dot{t}^2 + \frac{\dot{r}^2}{f(r)} = 0 \tag{4.8}$$

[4]The embedding into complex time can be repeated infinitely in both directions, by shifting t_E appropriately, as one crosses each horizon.

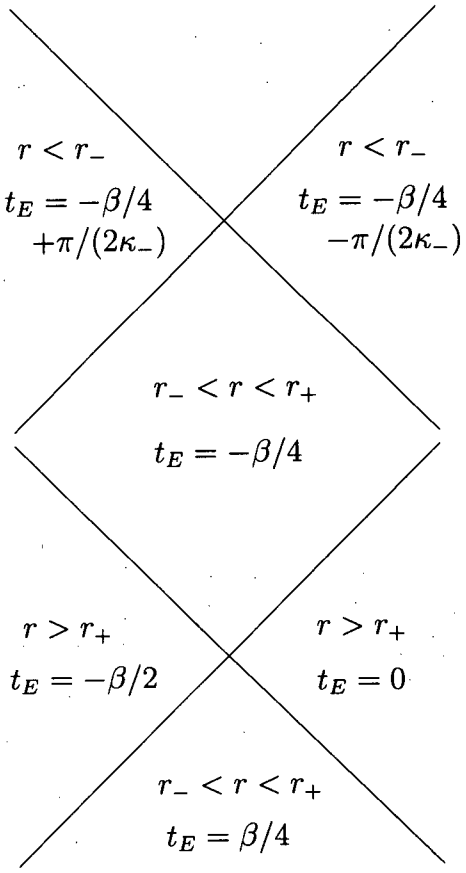

Figure 4.1: **The embedding into complex Schwarzschild time, showing the constant imaginary parts of $t = t_L + it_E$.**

where dots denote differentiation with respect to the affine parameter λ. There is a conserved energy, E, associated with the Killing vector $\partial/\partial t$, in terms of which the geodesic equations become

$$\dot{t} = \frac{E}{f(r)}, \qquad \dot{r}^2 = E^2. \tag{4.9}$$

For ingoing geodesics which start at the boundary $r = \infty$ at $t = 0$, the time t as a function of r is given by

$$t(r) = \int_r^\infty \frac{\mathrm{d}r'}{f(r')} = \int_{r^2}^\infty \frac{\mathrm{d}x}{2} \frac{x^{3/2}}{(x+x_0)(x-x_-)(x-x_+)}. \tag{4.10}$$

Explicitly, for $r < r_-$,

$$\begin{aligned} t(r) \;=\; & -\frac{x_0^{3/2}}{(x_0+x_-)(x_0+x_+)}\left(\tan^{-1}\left(\frac{r}{r_0}\right) - \frac{\pi}{2}\right) - \frac{1}{\kappa_-}\tanh^{-1}\left(\frac{r}{r_-}\right) \\ & + \frac{1}{\kappa_+}\tanh^{-1}\left(\frac{r}{r_+}\right) - \frac{i\pi}{2}\left(\frac{1}{\kappa_+} - \frac{1}{\kappa_-}\right) \end{aligned} \tag{4.11}$$

where the pure imaginary terms arise from integrating over the two poles at $x = x_\pm$. These are just the shifts in t_E discussed above. Such a geodesic will reach the singularity $r = 0$ at a finite time

$$t_{\text{sing}} = \frac{\pi}{2}\frac{x_0^{3/2}}{(x_0+x_-)(x_0+x_+)} - \frac{i\pi}{2}\left(\frac{1}{\kappa_+} - \frac{1}{\kappa_-}\right). \tag{4.12}$$

whose real part is positive. Conversely, a geodesic which hits the singularity at $t_L = 0$, must leave the boundary at time

$$t_c = -\frac{\pi}{2}\frac{x_0^{3/2}}{(x_0+x_-)(x_0+x_+)} < 0, \tag{4.13}$$

from which we conclude that one cannot draw both the boundaries and the singularities as straight lines in the Penrose diagram. Choosing the boundaries to be straight lines, then the singularities must be *bowed out*, the situation demonstrated in figure 4.2. However, it will become clear that this behaviour has no influence on the boundary theory. In particular the critical value t_c in the Schwarzschild case of [9] plays no role in the discussion of correlation functions here.

Kruskal Coordinates

As in the asymptotically flat case [30], we need two Kruskal-like coordinates patches to cover the region $0 < r < \infty$, one being valid through the outer horizon, the other being valid through the inner horizon. In the usual way, we first define the tortoise coordinate

$$r_* = \int_0^r \frac{\mathrm{d}r'}{f(r')} + C = x_0' \tan^{-1}\left(\frac{r}{r_0}\right) + \frac{1}{2\kappa_+}\ln\left(\frac{r-r_+}{r+r_+}\right) - \frac{1}{2\kappa_-}\ln\left(\frac{r-r_-}{r+r_-}\right) \tag{4.14}$$

where $x_0' = x_0^{3/2}/((x_0+x_+)(x_0+x_-))$ and we have chosen the constant C so as to make r_* real for $r > r_+$. As we cross the horizons from this region, we pick up the same constant imaginary terms as in the expression (4.11) for t, giving an embedding of the spacetime into the complex coordinate plane.

To cover the entire range of r, define the light cone coordinates $u = t - r_*, v = t + r_*$. For $r > r_-$, transform according to

$$U^+ = -e^{-\kappa_+ u} = T^+ - X^+, \qquad V^+ = e^{+\kappa_+ v} = T^+ + X^+ \tag{4.15}$$

whereas for $r < r_+$, take

$$U^- = -e^{+\kappa_- u} = T^+ - X^+, \qquad V^- = e^{-\kappa_- v} = T^- + X^-. \tag{4.16}$$

The outer horizon is given by $T^{+2} - X^{+2} = 0$ and the inner has $T^{-2} - X^{-2} = 0$. The metric becomes

$$\mathrm{d}s^2 = \frac{1}{\kappa_\pm^2} f(r)\, e^{\mp 2\kappa_\pm r_*}(-(\mathrm{d}T^\pm)^2 + (\mathrm{d}X^\pm)^2), \tag{4.17}$$

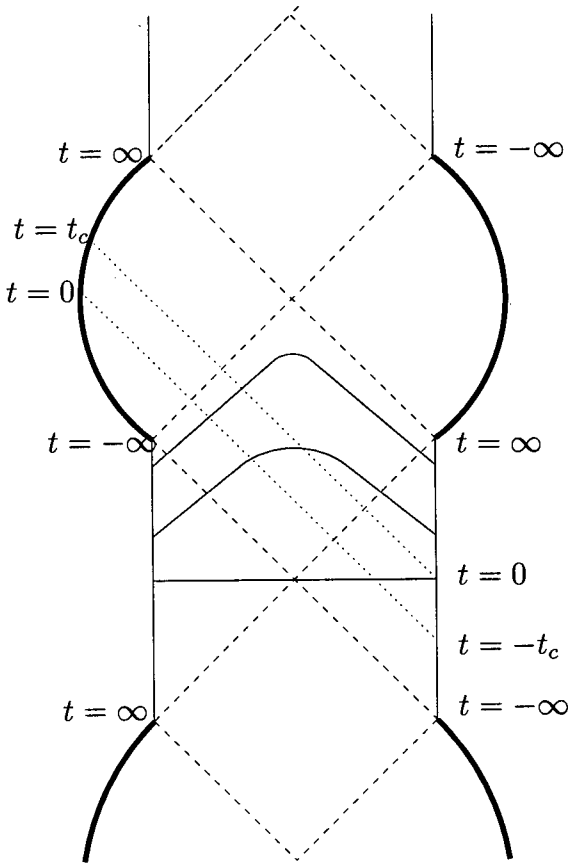

Figure 4.2: **The Penrose diagram repeats itself in both directions.** Radial null geodesics are dotted red, radial spacelike geodesics are solid blue, the inner and outer horizons are dashed and the singularities are bold. We have chosen to draw the boundaries as vertical lines, in which case the singularities are bowed out. The values of t all denote those of t_L, the real part of complex time.

where for $r > r_-$, $r(T^+, X^+)$ is determined implicitly by

$$T^{+2} - X^{+2} = -e^{2\kappa_+ r_*} = -e^{2\kappa_+ x_0' \tan^{-1}(r/r_0)} \left(\frac{r - r_+}{r + r_+}\right) \left(\frac{r + r_-}{r - r_-}\right)^{\kappa_+/\kappa_-} \tag{4.18}$$

and for $r < r_+$, $r(T^-, X^-)$ is determined by

$$T^{-2} - X^{-2} = -e^{-2\kappa_- r_*} = -e^{-2\kappa_- x_0' \tan^{-1}(r/r_0)} \left(\frac{r_+ + r}{r_+ - r}\right)^{\kappa_-/\kappa_+} \left(\frac{r_- - r}{r_- + r}\right). \tag{4.19}$$

However, the boundaries and singularities are covered by different coordinate patches, which makes comparison of them impossible.

One can instead follow [30] and use the coordinates defined in (4.15) for the regions $r > r_+$ *and* $r < r_-$. In the region $r_- < r < r_+$, we instead define the light cone coordinates

$u = t + r_*, v = -(t - r_*)$ and use

$$U = e^{\kappa_+ u} = T - X, \qquad V = e^{\kappa_+ v} = T + X. \tag{4.20}$$

The metric can be written everywhere as

$$\mathrm{d}s^2 = \frac{|f(r)|}{\kappa_+^2} e^{-2\kappa_+ r_*}(-\mathrm{d}T^2 + \mathrm{d}X^2) \tag{4.21}$$

which is analytic except at the inner horizon $r = r_-$. The radial coordinate r is determined implicitly by

$$T^2 - X^2 = \mp e^{2\kappa_+ x_0' \tan^{-1}(r/r_0)} \left(\frac{|r - r_+|}{r + r_+}\right) \left(\frac{r + r_-}{|r - r_-|}\right)^{\kappa_+/\kappa_-} \tag{4.22}$$

the $\mp$ sign corresponding to the regions $r > r_+$ and $r < r_-$, and $r_- < r < r_+$, respectively.

Now we can compare the boundaries and singularities in the first set of coordinates. In the limits

$$r \to \infty \quad \Rightarrow \quad T^2 - X^2 \to -e^{\pi\kappa_+ x_0'} < -1, \tag{4.23}$$

$$r \to 0 \quad \Rightarrow \quad T^2 - X^2 \to -1 \tag{4.24}$$

so in a (T, X) spacetime diagram, the hyperboli representing the singularities will be further away from the origin than the hyperboli representing the boundaries. This is opposite to the Schwarzschild case [9]. Following those arguments, one sees that on the resulting Penrose diagram if we draw the singularity $r = 0$ as a vertical line, the boundary $r = \infty$ must be bowed out. Alternatively, we can use a conformal transformation to make the singularity bowed out while keeping the boundary vertical. The latter case is shown schematically in figure 4.2. (In this case, to bring the boundaries of the spacetime to a finite coordinate distance we can, for example, let $U = e^{\pi\kappa_+ x_0'/2} \tan\tilde{u}$ and $V = e^{\pi\kappa_+ x_0'/2} \tan\tilde{v}$.)

4.2 Neutral Correlation Functions

We now discuss features of correlation functions of operators which are electrically neutral. When we put insertions on both boundaries, the correlation functions are dominated (in the limit of high dimensional operators) by spacelike geodesics, as was explained in [11]. Such geodesics are only sensitive to the metric, and not to the background electric field. In the present section, we can restrict ourselves to symmetric geodesics (which reach the boundaries at the same value of $t_L = t_0$), since all others can be obtained by time translation.

It is instructive to compare our discussion to that of the neutral black hole in [9]. The geometry in that case contains a singularity, which results in a specific feature of the geodesics – the regularised length goes to $-\infty$ at finite boundary time, and therefore the corresponding correlator diverges. This is incompatible with the structure of field theory correlation functions, which can be shown to be bounded (by their values at $t_L = 0$).

Luckily, one can also show by analysis of the Euclidean slice of the geometry that at $t_L = 0$ the correlators are dominated by complex geodesics, and the real geodesic is subdominant. It is therefore plausible that for any value of t_L the correlator is given by the same linear combination of the complex geodesics, thus avoiding the contradiction. The signature of the bulk singularity is then seen in an appropriate analytic continuation of the field theory results.

The two motivations for that conclusion are absent for near-extreme black holes. First, and for all black hole parameters, the region of our geometry which is probed by the geodesics is non-singular, and so the regularised length of the real geodesic behaves more sensibly – we will see that it is finite for any finite time, and goes to $+\infty$ at late boundary times, corresponding to a sensible exponential decay of the correlators at late time.

Secondly, for the near-extreme black holes, it will become clear that the correlators are bounded by their values at $t_L = 0$. The proper length of the relevant geodesic is a monotonically increasing function of energy, with minimum value at $E = 0$ (corresponding to $t_L = 0$). This is not the case for black holes far from extremality, however, and in that case we would expect the same subtleties of [9].

Finally, analysis of the Euclidean slice of the geometry reveals that for near-extreme black holes, the real geodesic dominates any complex ones, if such geodesics exist. It is then plausible that this real geodesic dominates the correlator at any t_L, in particular for late boundary time, setting the stage to use these geodesics to probe the structure of the perturbed spacetime.

We start in subsection 3.1 by discussing the qualitative features of the real geodesics, before presenting a more quantitative calculation of the correlation functions. As in the null case above, the geodesics are specified by the value of the energy E. In subsection 3.3, we turn to discussing in detail the relation between E and the boundary time, $t(E)$, and in subsection 3.4 we compute the length of the geodesics, which will determine the correlators in our approximation. We discuss the Euclidean slice of the geometry in subsection 3.4, showing that for appropriate black hole parameters the real geodesic dominates the correlation functions.

4.2.1 Qualitative Features

Radial Spacelike Geodesics

For radial spacelike geodesics, and normalizing appropriately, the Lagrangian is

$$\mathcal{L} = -f(r)\dot{t}^2 + \frac{\dot{r}^2}{f(r)} = 1. \tag{4.25}$$

The geodesic equations are

$$\dot{t} = \frac{E}{f(r)}, \qquad \dot{r}^2 = E^2 + f(r) \equiv E^2 - V(r), \tag{4.26}$$

the latter describing a particle of unit mass and of energy E^2 moving in an effective potential $V(r) = -f(r)$. General properties of the geodesics[5] can thus be read off from figure 4.3, in which the effective potential is shown.

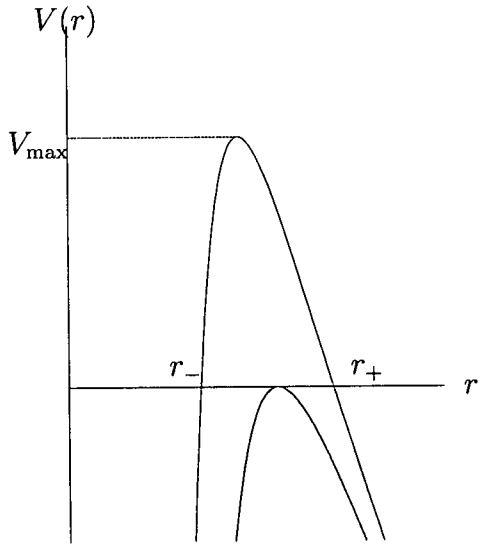

Figure 4.3: **The effective potential in the non-extreme case is shown in red, and the extreme case in blue.**

The extreme case is relatively uninteresting since there is no region between the horizon and the singularity which geodesics can probe. Geodesics with $E^2 > 0$ fall all the way into the singularity; those with $E^2 = 0$ reach the single event horizon before returning to the (same) boundary.

The non-extreme case has the following qualitative features:

- All geodesics with $E^2 \leq V_{\text{max}}$ return to the asymptotic region $r = \infty$, so will connect the two boundaries. The endpoints lie on the two opposite boundaries, as can be seen by inspecting $t(\lambda)$.
- Geodesics with $0 < E^2 \leq V_{\text{max}}$ will penetrate the outer horizon, and reach some minimal turning point between the two horizons. They cannot penetrate the inner horizon, and will in fact accumulate at some finite distance from it (the radius for which the potential attains its maximum V_{max}), as $E^2 \to V_{\text{max}}$.
- Geodesics with $E = V_{\text{max}}$ penetrate the furthest before returning to the boundary. These geodesics will turn out to have diverging boundary times.
- Geodesics with $E^2 > V_{\text{max}}$ will fall into the singularity, where our approximation breaks down. As the boundary time diverges before we reach this range of E^2, it seems that such trajectories do not contribute to any gauge theory process.

[5]The uncharged, non-rotating geodesics discussed here resemble geodesics in the AdS-Schwarzschild geometry which carry angular momentum [9].

Apparently, at least for the observables we are interested in, the region beyond the Cauchy horizon is not encoded in the gauge theory. Similar conclusions about three dimensional rotating black holes have been obtained in [15]. Moreover, the geodesics do not even reach the Cauchy horizon itself, reaching at most some minimal distance[6] from it. We will see later that, even when perturbing the spacetime, the observables of interest are screened from any dramatic behaviour associated with the Cauchy horizon by this geometrical effect.

Rotating Spacelike Geodesics

Let us add an angular momentum L, conjugate to the azimuthal angle ϕ on the boundary three-sphere[7]. It is the conserved quantity associated with the Killing vector $\partial/\partial\phi$, the relevant geodesic equation being

$$\dot{\phi} = \frac{L}{r^2}. \tag{4.27}$$

In this case, the effective potential is modified to $V(r) = -f(r)(1 - L^2/r^2)$ which, in addition to r_+ and r_-, has an additional root at $r = |L|$. A sketch of one possibility is given in figure 4.4.

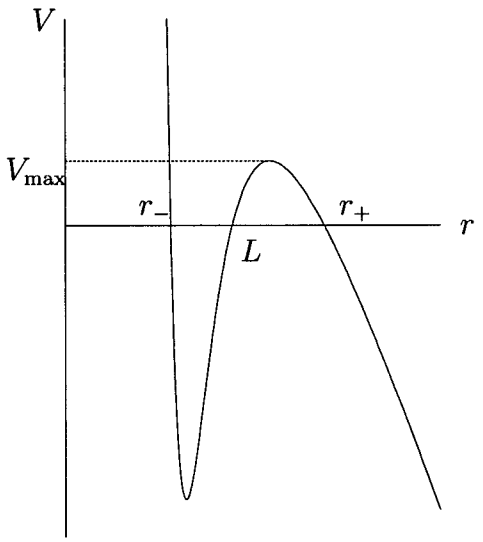

Figure 4.4: **The effective potential for a rotating geodesic with $x_- < L^2 < x_+$.** Other choices of the relative magnitude of L^2, x_- and x_+ simply switch the roots. If L^2 is equal to either x_- or x_+, then those two roots will coalesce. The local maximum $V_{\max}$ is also shown.

In the vicinity of the singularity at $r = 0$, the potential is very different to the non-rotating case: for an arbitrarily small angular momentum, it turns around at small values of r. Consequently, for sufficiently large E one can come arbitrarily close to the singularity and still return to the asymptotic region $r = \infty$; naively the corresponding two-sided correlators are sensitive to the region inside the inner horizon.

[6]This minimal distance can be large for far from extreme black holes, and goes to zero in the extreme limit.

[7]For more general rotation, one replaces L^2 by the relevant Casimir operator.

However, a closer inspection reveals that such geodesics are irrelevant for the two-sided correlators. Once again, as $E^2 \to V_{\max}$, the boundary time diverges. In addition, the behaviour of $t(\lambda)$ shows that these geodesics connect two boundary points on the *same* side of the Penrose diagram. It is not clear what role, if any, such components play in the field theory dual, since inner horizon instabilities are likely to change the causal structure and eliminate these additional boundaries.

The qualitative details of the rotating trajectories with $E^2 \leq V_{\max}$ depend only on the relative values of r_+ and L. For $|L| > r_+$ the geodesics do not penetrate the outer horizon, making them uninteresting for our purposes. On the other hand, for $|L| < r_+$ the situation is basically unchanged from the non-rotating case, the geodesics for which $0 < E^2 \leq V_{\max}$ being relevant to us.

4.2.2 Boundary Time

In this subsection we describe the relation between (the real part of) the boundary time t_0 and the energy E. We are interested in symmetric geodesics which start at a point t_0 on the boundary, and end at the point $-(t_0 + i\beta/2)$ on the other boundary. Taking r_E to denote the turning point for a trajectory of energy E^2, we have

$$E^2 + f(r_E) = 0. \tag{4.28}$$

As in [9], we must have $t_L(r_E) = 0$ and $t_E(r_E) = -\beta/4$. Such geodesics satisfy

$$t_0 + i\frac{\beta}{4} = E\int_{r_E}^{\infty} \frac{\mathrm{d}r}{V(r)\sqrt{E^2 - V(r)}} \tag{4.29}$$

where $V(r)$ is the effective potential described above, for either rotating or non-rotating geodesics. Since the qualitative features are similar, we will only be concerned with the latter, for which $V(r) = -f(r)$.

The two features prominent in the analogous discussion of [9], for the AdS-Schwarzschild metric, are the branch cut at $t_0 = 0$ (corresponding to $E = 0$) and the existence of a critical value $t_0 = -t_c$ (corresponding to $E = \infty$), where the correlators naively diverge. The latter feature was interpreted as a signal of the singularity encoded in gauge theory correlation functions, the former making that encoding a subtle one. In our discussion these features are no longer present. The special values of the energy are $E = 0$ and $E^2 = V_{\max}$, and we discuss them both below.

For general energies, one can compute (4.29) in terms of elliptic integrals[8], which we do in the appendix. The result will depend both on the roots of the cubic $\Delta(x)$ and on the roots of the other cubic appearing in the denominator of (4.29),

$$\tilde{\Delta}(x) = E^2x^2 + (x + x_0)(x - x_-)(x - x_+) \equiv (x + \tilde{x}_0)(x - \tilde{x}_-)(x - \tilde{x}_+) \tag{4.30}$$

where the roots $\tilde{x}_+ > \tilde{x}_- > 0 > -\tilde{x}_0$ and $\tilde{x}_+ = r_E^2$.

[8]We use the notation of [31] for the elliptic integrals.

From the appendix (B), we have[9]

$$t_0 = -E\frac{1}{\sqrt{\tilde{x}_+(\tilde{x}_- + \tilde{x}_0)}}\left[\frac{x_0^3(\tilde{x}_+ - \tilde{x}_-)}{(\tilde{x}_+ + x_0)(\tilde{x}_- + x_0)(x_0 + x_-)(x_0 + x_+)}\,\Pi(\tilde{\phi}, \tilde{\alpha}_0^2, \tilde{k})\right.$$
$$+\frac{x_-^3(\tilde{x}_+ - \tilde{x}_-)}{(\tilde{x}_+ - x_-)(\tilde{x}_- - x_-)(x_0 + x_-)(x_+ - x_-)}\,\Pi(\tilde{\phi}, \tilde{\alpha}_-^2, \tilde{k})$$
$$-\frac{x_+^3(\tilde{x}_+ - \tilde{x}_-)}{(\tilde{x}_+ - x_+)(\tilde{x}_- - x_+)(x_0 + x_+)(x_+ - x_-)}\,\Pi(\tilde{\phi}, \tilde{\alpha}_+^2, \tilde{k})$$
$$\left.+\frac{\tilde{x}_-^3}{(\tilde{x}_- + x_0)(\tilde{x}_- - x_-)(\tilde{x}_- - x_+)}\,\mathrm{F}(\tilde{\phi}, \tilde{k})\right] \tag{4.31}$$

where

$$\tilde{\alpha}_0^2 = \left(\frac{\tilde{x}_+ + \tilde{x}_0}{\tilde{x}_- + \tilde{x}_0}\right)\left(\frac{\tilde{x}_- + x_0}{\tilde{x}_+ + x_0}\right), \qquad \tilde{\alpha}_-^2 = \left(\frac{\tilde{x}_+ + \tilde{x}_0}{\tilde{x}_- + \tilde{x}_0}\right)\left(\frac{\tilde{x}_- - x_-}{\tilde{x}_+ - x_-}\right),$$
$$\tilde{\alpha}_+^2 = \left(\frac{\tilde{x}_+ + \tilde{x}_0}{\tilde{x}_- + \tilde{x}_0}\right)\left(\frac{\tilde{x}_- - x_+}{\tilde{x}_+ - x_+}\right), \qquad \tilde{k} = \sqrt{\frac{\tilde{x}_-}{\tilde{x}_+}\left(\frac{\tilde{x}_+ + \tilde{x}_0}{\tilde{x}_- + \tilde{x}_0}\right)}, \qquad \tilde{\phi} = \sin^{-1}\sqrt{\frac{\tilde{x}_- + \tilde{x}_0}{\tilde{x}_+ + \tilde{x}_0}}. \tag{4.32}$$

Note that this result includes the imaginary part $-i\beta/4$ from crossing the horizon; it arises from a pole in the region of integration in the third term above.

This is a fairly unilluminating expression, but more information can be seen if we plot $t(E)$ numerically, for various choices of black hole parameters. We find two distinct types of behaviour, shown in figure 4.5:

- The left-hand plot is representative of the behaviour for $x_+ \sim x_-$, where the black hole is near-extreme. The boundary time t is then a monotonically increasing function of energy E.
- The right-hand plot, on the other hand, represents the behaviour for $x_+ >> x_-$, this limit being one of large mass and small charge.
- In both cases, we clearly see a divergence in t as $E^2 \to V_{\max}$.

There is thus a range of parameter space in which, for each value of boundary time t, there exists a unique geodesic connecting the two boundary points (the left-hand plot in figure 4.5). However, outside of this range (the right-hand plot in figure 4.5), there are values of boundary time for which there are multiple geodesics connecting the two boundaries, each with a different value of E. Which one dominates the path integral will depend on the relative proper lengths, though one should be more careful than this: some of these saddle points may not contribute to the path integral at all.

[9]This expression is actually valid for *any* geodesic, not just symmetric ones. We simply have to replace t_0 with $t_{\mathrm{b}} - t_{\mathrm{tp}}$, these values denoting, respectively, the values of t_L at the boundary and at the turning point.

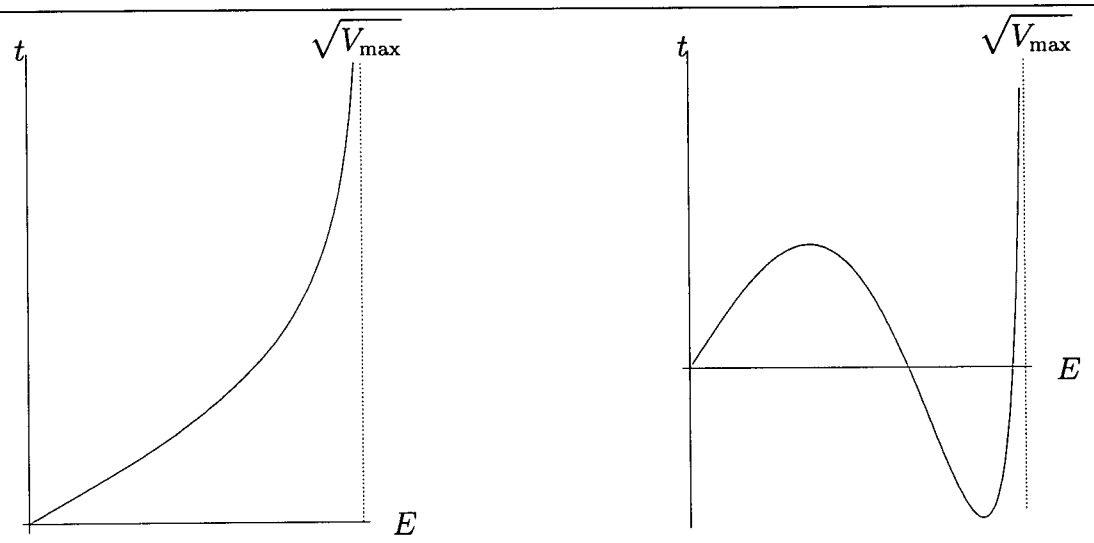

Figure 4.5: **The behavior of boundary time as a function of energy.** The left-hand plot shows $t(E)$ for $x_+ \sim x_-$ whereas the right-hand plot has $x_+ >> x_-$. The dotted lines indicate $E^2 = V_{max}$.

The precise point of cross-over between these two types of behaviour, as a function of parameters, is difficult to pin down analytically but is possible to analyse numerically. For example, figure 4.6 shows a region of $x_\pm$ parameter space, the circles denoting that t is a monotonically increasing function of E for those choices of parameters, and the crosses denoting that t has a turning point[10].

It should be clear from this figure that the near-extreme black holes have unique geodesics connecting boundary points, the boundary time t in this case being a single-valued function of the energy E.

Small E Geodesics

It is easy to see that $E = 0$ corresponds to $t_0 = 0$, both for rotating and non-rotating geodesics. For $E = 0$, we have

$$\dot{t} = 0 \qquad \Rightarrow \qquad t(\lambda) = 0, \qquad \dot{r}^2 = f(r), \tag{4.33}$$

so these geodesics start at the boundary, pass straight through the Penrose diagram and end at the other boundary, without ever penetrating the horizon.

To derive the small E behaviour of (4.31), we need the E-dependence of the roots $\tilde{x}_0, \tilde{x}_-$ and $\tilde{x}_+$. This is determined by the following set of equations:

$$\begin{aligned} &\tilde{x}_0 - \tilde{x}_- - \tilde{x}_+ = x_0 - x_- - x_+ + E^2, \\ &\tilde{x}_-\tilde{x}_+ - \tilde{x}_0\tilde{x}_+ - \tilde{x}_0\tilde{x}_- = x_-x_+ - x_0x_+ - x_0x_-, \\ &\tilde{x}_0\tilde{x}_-\tilde{x}_+ = x_0x_-x_+. \end{aligned} \tag{4.34}$$

[10]It is curious that the boundary between these two types of behaviour is a straight line.

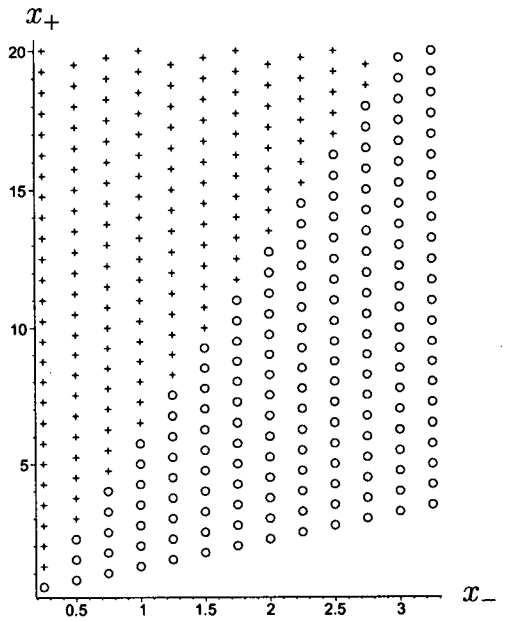

Figure 4.6: **This plot shows how $t(E)$ behaves as a function of the parameters $x_\pm$.** Circles denote points for which t is a monotonically increasing function of E, and crosses denote points for which t has a turning point for some value of E.

Since we are interested only in small E, we can solve these by taking

$$\begin{aligned} \tilde{x}_0 &= x_0 + (1 + a_- + a_+)E^2 + \mathcal{O}(E^4), \\ \tilde{x}_- &= x_- + a_- E^2 + \mathcal{O}(E^4), \\ \tilde{x}_+ &= x_+ + a_+ E^2 + \mathcal{O}(E^4) \end{aligned} \tag{4.35}$$

where

$$a_\pm = \mp \frac{r_\pm}{\kappa_\pm}. \tag{4.36}$$

It is important that the possible order E terms in (4.35) necessarily vanish, as long as $x_+ \neq x_-$, which in turn implies that all odd powers of E also vanish. We then have

$$\tilde{\phi} = \phi + \phi_1 E^2 + \mathcal{O}(E^4), \qquad \tilde{k} = k + k_1 E^2 + \mathcal{O}(E^4), \qquad \tilde{\alpha}^2 = \alpha^2 + \alpha_1^2 E^2 + \mathcal{O}(E^4) \tag{4.37}$$

(for each of the $\tilde{\alpha}$s), and where the quantities without a tilde are independent of E, being functions of the roots x_0, x_- and x_+ only. The elliptic integrals can then be Taylor expanded in each of their arguments as

$$\begin{aligned} F(\tilde{\phi}, \tilde{k}) &= F(\phi, k) + E^2 \left(\phi_1 \frac{\mathrm{d}F}{\mathrm{d}\phi} + k_1 \frac{\mathrm{d}F}{\mathrm{d}k} \right) + \mathcal{O}(E^4), \\ \Pi(\tilde{\phi}, \tilde{\alpha}^2, \tilde{k}) &= \Pi(\phi, \alpha^2, k) + E^2 \left(\phi_1 \frac{\mathrm{d}\Pi}{\mathrm{d}\phi} + k_1 \frac{\mathrm{d}\Pi}{\mathrm{d}k} + \alpha_1^2 \frac{\mathrm{d}\Pi}{\mathrm{d}(\alpha^2)} \right) + \mathcal{O}(E^4) \end{aligned} \tag{4.38}$$

using the well-known expressions for the various derivatives [31].

The explicit expressions quickly become complicated and rather un-illuminating, but

the net result is that

$$t_0 = t_1 E + \mathcal{O}(E^3) \tag{4.39}$$

for some non-vanishing constant t_1. This expression for $t(E)$ is similar to the finite mass black hole of [9], and in particular is an analytic function near $E = 0$. Moreover, numerical experimentation shows (as in figure 4.5) that for generic choices of the black hole parameters, the constant $t_1 > 0$. We can generate cases for which $t_1 < 0$, for example by taking $x_- = 0.2$ and $x_+ = 1$, but we have to work quite hard to do this: it seems that we need x_- small. This is just the Schwarzschild limit $x_- \to 0$ and, in that case, we can find both small and large mass (small and large x_+) black holes with $t_1 < 0$. So, although there are black holes with $t_1 < 0$, they are all in the neighbourhood of the neutral hole; we will concentrate on the generic case with $t_1 > 0$.

The Regime $E^2 \to V_{\max}$

The integrand in (4.29) is divergent at the turning point of the trajectory, where $E^2 = V(r)$. This singularity is integrable for $E^2 \neq V_{\max}$, leading to finite boundary time t_0 for $0 < E^2 < V_{\max}$. On the other hand, when $E^2 = V_{\max}$, the two positive roots of $\tilde{\Delta}(x)$ coincide ($\tilde{x}_+ = \tilde{x}_-$), leading to a logarithmic divergence in (4.29). We emphasise that this is true for both the rotating and non-rotating geodesics.

The divergence is shown clearly in figure 4.5, but we can see it analytically from the exact result (4.31) in the following way. Take $\tilde{x}_- = \tilde{x}_+ - \varepsilon$ and note that $\tilde{k}$ and each $\tilde{\alpha}^2$ go to one faster than $\tilde{\phi}$ goes to $\pi/2$, since

$$\tilde{k} = 1 + \mathcal{O}(\varepsilon), \qquad \tilde{\alpha}^2 = 1 + \mathcal{O}(\varepsilon), \qquad \tilde{\phi} = \frac{\pi}{2} + \mathcal{O}(\varepsilon^{1/2}). \tag{4.40}$$

Then note that

$$\tilde{x}_+ - \tilde{x}_- = \frac{\tilde{x}_+(\tilde{x}_- + \tilde{x}_0)}{\tilde{x}_0}(1 - \tilde{k}^2) \tag{4.41}$$

and use [31]

$$\Pi(\phi, 1, k) = \frac{1}{(1-k^2)}\left((1-k^2)\,F(\phi,k) - E(\phi,k) + \tan\phi\sqrt{1 - k^2\sin^2\phi}\right). \tag{4.42}$$

The problematic $(1 - k^2)$ factors cancel, giving

$$\begin{aligned} t_0 &= -E\frac{\tilde{x}^{5/2}}{(\tilde{x}_+ + \tilde{x}_0)^{3/2}(\tilde{x}_+ - x_-)(\tilde{x}_+ - x_+)}\ln(\tan\tilde{\phi} + \sec\tilde{\phi}) \\ &\sim -\ln(\cos\pi/2) + \text{finite}, \end{aligned} \tag{4.43}$$

since $x_- < \tilde{x}_+ < x_+$.

Since the boundary time diverges as $E^2 \to V_{\max}$, the gauge theory does not seem to encode the regime $E^2 > V_{\max}$.

4.2.3 Correlation Functions

The proper length of both the rotating and non-rotating geodesics is given by

$$L = 2\int_{r_E}^{r_{\max}} \frac{\mathrm{d}r}{\sqrt{E^2 - V(r)}} \tag{4.44}$$

with $V(r)$ being the relevant potential in each case. r_E is the same turning point as in the previous subsection and, since we will only be concerned with the non-rotating case, it is again given by solving (4.28). The upper limit, $r_{\max}$, is a long-distance radial cutoff, dual to the UV cutoff in the gauge theory. As we take $r_{\max} \to \infty$, the integral diverges logarithmically. To regularise it we subtract the divergent piece arising in the pure AdS case (obtained by setting $x_0 = 1$ and $x_- = x_+ = 0$ in the above expression). This standard process is dual to renormalisation of the boundary theory [32].

$E = 0$ Geodesics

We start with the $E = 0$ symmetric geodesics, which approximate the boundary correlators with $t_0 = 0$. The proper length of such a geodesic is

$$L = 2\int_{r_+}^{r_{\max}} \frac{\mathrm{d}r}{\sqrt{f(r)}} = \int_{r_+^2}^{r_{\max}^2} \mathrm{d}x \sqrt{\frac{x}{(x+x_0)(x-x_-)(x-x_+)}} \tag{4.45}$$

where the turning point for $E = 0$ is $r = r_+$, the location of the outer horizon. We can compute (4.45) in terms of elliptic integrals, giving [31]

$$L = \frac{2}{\sqrt{x_+(x_- + x_0)}} \left[x_-\, \mathrm{F}(\phi, k) + (x_+ - x_-)\, \Pi(\phi, x_+k^2/x_-, k)\right] \tag{4.46}$$

where

$$\phi = \sin^{-1}\sqrt{\frac{(x_- + x_0)(r_{\max}^2 - x_+)}{(x_+ + x_0)(r_{\max}^2 - x_-)}}, \qquad k = \sqrt{\frac{x_-(x_+ + x_0)}{x_+(x_- + x_0)}} = \sqrt{\frac{\kappa_+}{\kappa_-}\frac{r_+}{r_-}}. \tag{4.47}$$

In the limit $r_{\max} \to \infty$, the logarithmic divergence appears in $\Pi(\phi, x_+k^2/x_-, k)$ (whereas $\mathrm{F}(\phi, k)$ remains finite). To extract this divergence, we note that $\alpha^2 = x_+k^2/x_- > 1$, so we can use [33]

$$\Pi(\phi, \alpha^2, k) = -\Pi(\phi, k^2/\alpha^2, k) + \mathrm{F}(\phi, k) + \frac{1}{2p_1}\ln\left(\frac{\Delta(\phi) + p_1\tan\phi}{\Delta(\phi) - p_1\tan\phi}\right) \tag{4.48}$$

where $p_1 = \sqrt{(\alpha^2 - 1)(1 - k^2/\alpha^2)}$ and $\Delta(\phi) = \sqrt{1 - k^2\sin^2\phi}$. Expanding to first order in $1/r_{\max}^2$ gives

$$L = \frac{2}{\sqrt{x_+(x_- + x_0)}} \left[x_+\, \mathrm{F}(\phi, k) - (x_+ - x_-)\, \Pi(\phi, x_-/x_+, k)\right] + \ln\left(\frac{4}{x_0 + x_- + x_+}\right) + \ln(r_{\max}^2), \tag{4.49}$$

the logarithmic divergence being manifest. The renormalised result is thus

$$L_{\text{ren}} = \frac{2}{\sqrt{x_+(x_- + x_0)}} \left[x_+ \, \mathrm{F}(\phi, k) - (x_+ - x_-) \, \Pi(\phi, x_-/x_+, k)\right] + \ln\left(\frac{4}{x_0 + x_- + x_+}\right) \tag{4.50}$$

where now

$$\phi = \sin^{-1}\sqrt{\frac{x_- + x_0}{x_+ + x_0}}. \tag{4.51}$$

$0 < E < V_{\text{max}}$ Geodesics

As in [9], as we increase the energy, the geodesic will penetrate some distance inside the horizon. The proper length of the (non-rotating) geodesic is now:

$$L = 2\int_{r_E}^{r_{\text{max}}} \frac{\mathrm{d}r}{\sqrt{E^2 + f(r)}} = \int_{r_E^2}^{r_{\text{max}}^2} \mathrm{d}x \sqrt{\frac{x}{E^2x^2 + (x + x_0)(x - x_-)(x - x_+)}} \tag{4.52}$$

which will depend on the roots of the cubic $\tilde{\Delta}(x)$, defined in (4.30). Formally, the result is as in (4.50), but with the E-dependent roots:

$$L_{\text{ren}} = \frac{2}{\sqrt{\tilde{x}_+(\tilde{x}_- + \tilde{x}_0)}} \left[\tilde{x}_+ \, \mathrm{F}(\tilde{\phi}, \tilde{k}) - (\tilde{x}_+ - \tilde{x}_-) \, \Pi(\tilde{\phi}, \tilde{x}_-/\tilde{x}_+, \tilde{k})\right] + \ln\left(\frac{4}{\tilde{x}_0 + \tilde{x}_- + \tilde{x}_+}\right) \tag{4.53}$$

where

$$\tilde{\phi} = \sin^{-1}\sqrt{\frac{\tilde{x}_- + \tilde{x}_0}{\tilde{x}_+ + \tilde{x}_0}}, \qquad \tilde{k} = \sqrt{\frac{\tilde{x}_-(\tilde{x}_+ + \tilde{x}_0)}{\tilde{x}_+(\tilde{x}_- + \tilde{x}_0)}}. \tag{4.54}$$

To take the small E limit of this expression, we proceed as in the previous subsection, using the expressions (4.35). The upshot is that

$$L(E) - L(E = 0) = L_1 E^2 + \mathcal{O}(E^4) \tag{4.55}$$

for some non-vanishing constant L_1. Using the previous expression (4.39) for the small E behaviour of the boundary time, we see that

$$L(E) - L(E = 0) \sim t^2. \tag{4.56}$$

The result is therefore analytic around $E = 0$, the branch cut structure found in [9] for the infinitely massive black hole being absent here. It is more similar to the finite mass black hole [9].

On the other hand, as for the computation of the boundary time above, the integral (4.44) will have an additional logarithmic divergence at the lower limit for $E = V_{\text{max}}$, which we can again extract analytically, or observe numerically. In figure 4.7, we plot $L(E)$, the proper length as a function of energy, for the two different regimes of the previous subsection. The parameters are the same as those in figure 4.5, the left-hand plot being representative of the behaviour for $x_+ \sim x_-$, and the right-hand plot being representative

of the behaviour for $x_+ >> x_-$. The divergence as $E^2 \to V_{\max}$ can clearly be seen. We emphasize again that the regularized length diverges to $+\infty$, and correspondingly the correlators *decay* exponentially.

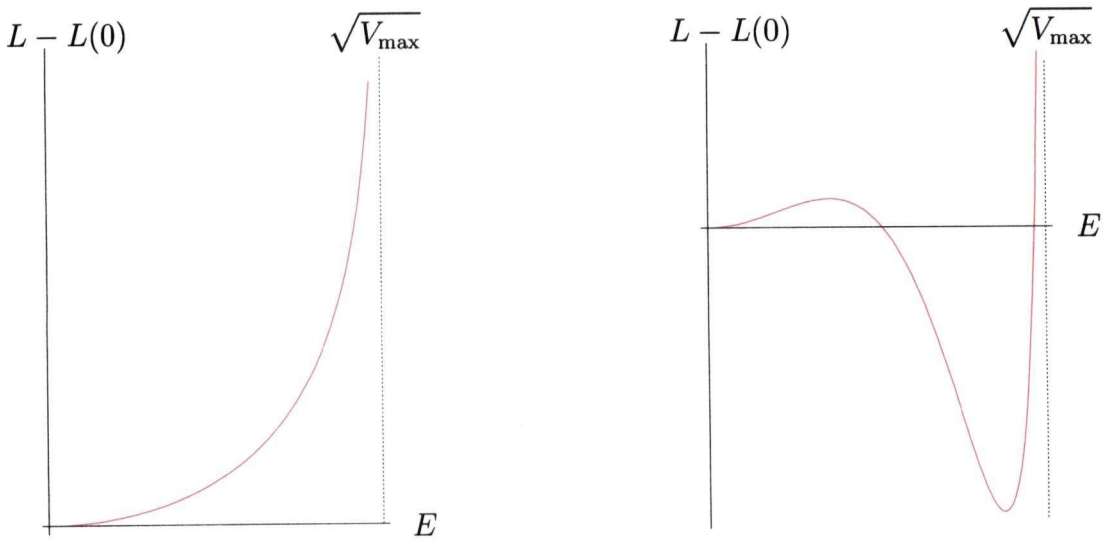

Figure 4.7: **The behavior of proper length of the spacelike geodesics as a function of energy.** The left-hand plot shows $L(E) - L(E = 0)$ for $x_+ \sim x_-$ whereas the right-hand plot has $x_+ >> x_-$. The dotted lines indicate $E^2 = V_{\max}$.

There are two important points to note here. Firstly, as shown in figure 4.7, for generic choices of black hole parameters, we have the constant $L_1 > 0$ in the small E behaviour (4.55). As for the small E behaviour of the boundary time, however, it is possible to arrange that $L_1 < 0$. But, again, these cases seem non-generic and we will concentrate on black holes with $L_1 > 0$. (The black holes in the Schwarschild limit $x_- \to 0$, with $t_1 < 0$ in (4.39), also have $L_1 < 0$ in (4.55).)

In that case, and for near-extreme black holes, it should be clear that the correlator will be bounded by its value at $t_L = 0$. The left-hand plot in figure 4.7 shows in this case that L is a monotonically increasing function of E, its minimum value indeed being at $E = 0$ (and so at $t_L = 0$). So, at least in this case, there is no contradiction with our field theory intuition. For the black holes far from extremality, however, this is no longer clear, as the right-hand plot in figure 4.7 shows. As in the neutral case [9], one would have to be more careful to reconcile our plots with the field theory properties.

We will thus concentrate on the generic near-extreme black holes, and have these in mind when we turn to analyse the perturbed spacetimes. Moreover, as we will see in the following subsection, it is indeed the real geodesics that dominate the late time correlators for these near-extreme black holes.

4.2.4 Euclidean Slice

Here we want to show that the real geodesics discussed above dominate the correlation function at $t_L = 0$. We can then plausibly argue, as in [9], that the real geodesics continue

to dominate at late times. We will not comment on the subtleties of analytic continuation from the Euclidean regime, but we will show – at least for certain choices of black hole parameters – that the real geodesic at $t_L = 0$ has shorter proper length than the complex goedesics, and should thus dominate the correlator.

The Euclidean metric is found in the usual way, by setting $t = it_E$. With respect to the geodesics, the effect is simply to take $E = -i\tilde{E}$, where the "Euclidean energy" $\tilde{E}$ is the conserved quantity associated with t_E. It turns out that our expressions (4.31) and (4.53) for the boundary time and proper length are still valid after performing this analytic continuation, both on the explicit E dependence, and on that appearing in the expressions (4.34) for the E-dependent roots. We can then plot the boundary time $t_E(\tilde{E})$ and proper length $L(\tilde{E})$ in the Euclidean regime, as we did for the Lorentzian case above.

Before presenting these plots, let us analyse the expected small $\tilde{E}$ behaviour. We can derive this from an analytic continuation of the results (4.39) and (4.55) in the Lorentzian case, finding

$$t_E(\tilde{E}) = -t_1\tilde{E} + t_2\tilde{E}^3, \tag{4.57}$$

$$L(\tilde{E}) - L(0) = -L_1\tilde{E}^2 + L_2\tilde{E}^4. \tag{4.58}$$

We argued above that, for generic choices of black hole parameters, we have $t_1 > 0$ and $L_1 > 0$, but the signs of the next-to-leading-order terms are harder to determine. It appears that either sign for both t_2 and L_2 is possible, depending on the black hole parameters.

Either way, at large values of $\tilde{E}$ there is a unique goedesic for each value of t_E. As we decrease $\tilde{E}$, however, and come into the small $\tilde{E}$ domain, other geodesics might appear, as in [9]. From (4.57), it is clear that this will occur when $\tilde{E} \sim \sqrt{t_1/t_2}$. Since we have assumed $t_1 > 0$, we will only encounter a branch point when $t_2 > 0$. Otherwise, there will be a unique geodesic for all $\tilde{E} > 0$.

At precisely $t_E = 0$, there are three solutions of (4.57). We will have geodesics with either $\tilde{E} = 0$, or $\tilde{E} = \pm\sqrt{t_1/t_2}$. The former has zero proper length, and may or may not dominate over the latter two. However, if we consider black holes for which $t_2 < 0$ (and $t_1 > 0$) then we simply never encounter a branch point. There is only ever one branch and we can continue into the Lorentzian regime, by taking $t_L > 0$, moving along the single real branch of geodesics. On the other hand, in the case that $t_2 > 0$, the proper length of the two geodesics with non-zero $\tilde{E}$ is

$$L = \frac{1}{t_2^2}(L_2 - t_1 L_1 t_2), \tag{4.59}$$

so which geodesics dominate the correlator will depend on the specific values of the various constants.

The important point is that there are black holes with $t_2 < 0$, so that no branch points appear as we take $\tilde{E} \to 0$. We can see that such black holes exist by plotting the Euclidean boundary time $t_E(\tilde{E})$. We find that t_E is generically a single-valued function of $\tilde{E}$, as shown in figure 4.8, monotonically decreasing from its value $\beta/4$ at $\tilde{E} = 0$. This seems to be true for both near-extreme and far-from-extreme black holes. Other behaviour is possible, however, in that we can find parameters for which t_E is multi-valued. As for our

discussion of the small E behaviour in the previous two subsections, it seems that we have to take x_- small to arrange this. And, since taking $x_- \to 0$ is the Schwarzschild limit, we should not be surprised to find such behaviour, since this is what was found in [9]. Away from this limit, however, the picture should be clear.

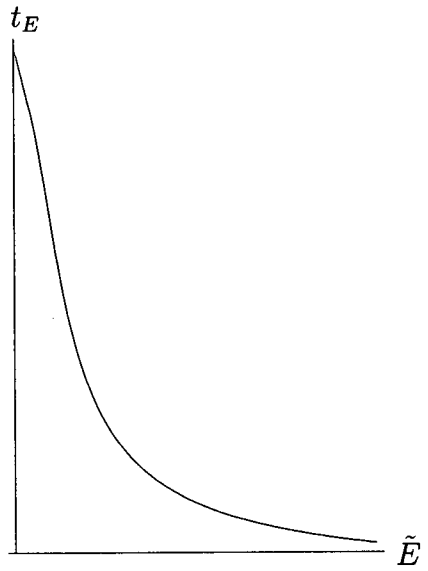

Figure 4.8: **A plot of the boundary time t_E in the Euclidean regime, with $x_- = 1, x_+ = 4$.** At $\tilde{E} = 0$ we have $t_E = \beta/4$. This type of behaviour – the fact that t_E is single-valued – seems fairly generic.

In fact, we have the stronger result that t_E is generically single-valued for *most* values of $\tilde{E}$, not just in the $\tilde{E} \to 0$ limit. In that case, there is no evident issue with complex branches, and the real geodesic will dominate the late time correlators. We note also that those conclusions hold for sufficiently small black hole, both for near-extremal and near-neutral ones.

It is helpful to have a look the behavior of $L(t)$, which can give us some idea of the dominance and the transition of geodesics. At first we just consider the real geodesics. Fixing one of the parameters x_-, we tune the other one x_+, which corresponds to the tuning of mass, charge of the black hole. In the figure 4.9 there exists a transition process of the geodesics. When the black hole is close to extreme case, it just has a real geodesic, while the parameters go to more neutral region, a pair of new real ones are created, and the dominance changes. (From the correlation function point of view, the geodesic with the smallest value of proper length dominates.)

Adding up the Euclidean slice will give us a more clear picture. As shown in figure 4.10, there is always a transition from a real geodesic to a Euclidean one, and for fixed parameters (x_-, x_+), the number of total geodesics seems conserved. And it is natural to conjecture that generally at the critical points where a pair of real geodesics are created, there are transitions between complex geodesics and the real. (We checked numerically when $t \gtrsim \tilde{t}$ in figure 4.9 there are two complex geodesics analytically continued from the real ones in $t \lesssim \tilde{t}$.) We are not sure whether the total number of geodesics are conserved

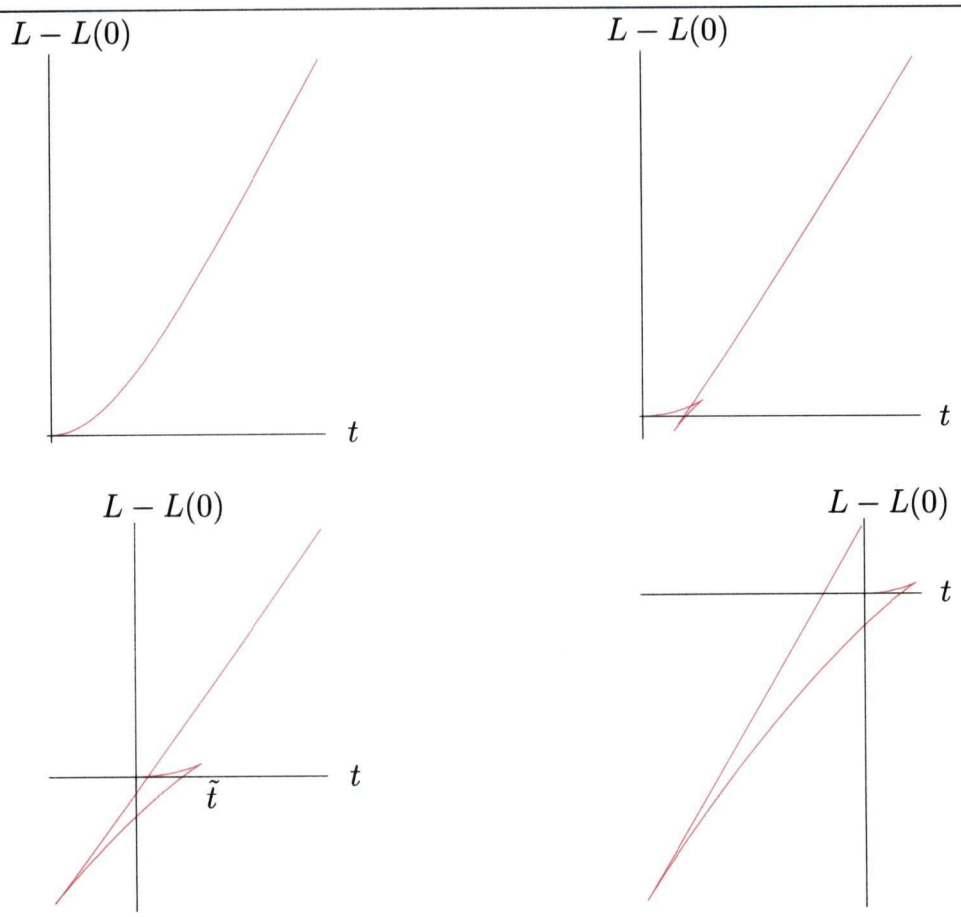

Figure 4.9: **Several real $L(t)$ graphs with the same x_- and different x_+.** The top left-hand plot shows $L(t)$ for the near extremal black hole, where there is no transition. The other plots show the case of first order behaviour discussed in the text, which exists far enough from extremality. The black hole is further from extremality as the plots are read from top left to top right, to bottom left to bottom right. $\tilde{t}$ in bottom left plot indicates the critical time of two real geodesics created.

for all cases, but it is much more possible that it is valid for fixed parameters. That is, if we have a specific AdS charged black hole, the total number of geodesics between two different boundaries is always the same, independent on the positions of boundary points we consider.

Another significant phenomenon is that the dominance relation can be different with a different set of parameters. In the right-top diagram of figure 4.10, a real geodesic dominates at $t = 0$, while in the bottom diagram, the pure Euclidean one dominates. This verifies the complexity again when the black hole is far away from the extreme case. Fortunately we can show that for most of the values of parameters, $L(t)$ has a single valued behavior, as in the left-top diagram. So we just constrain ourselves in such simple cases.

4.2.5 Behaviour at Finite t_L

We have found that the subtle features of the infinitely massive AdS-Schwarzschild black hole are likely to be absent in our calculation. This is not surprising, since even very

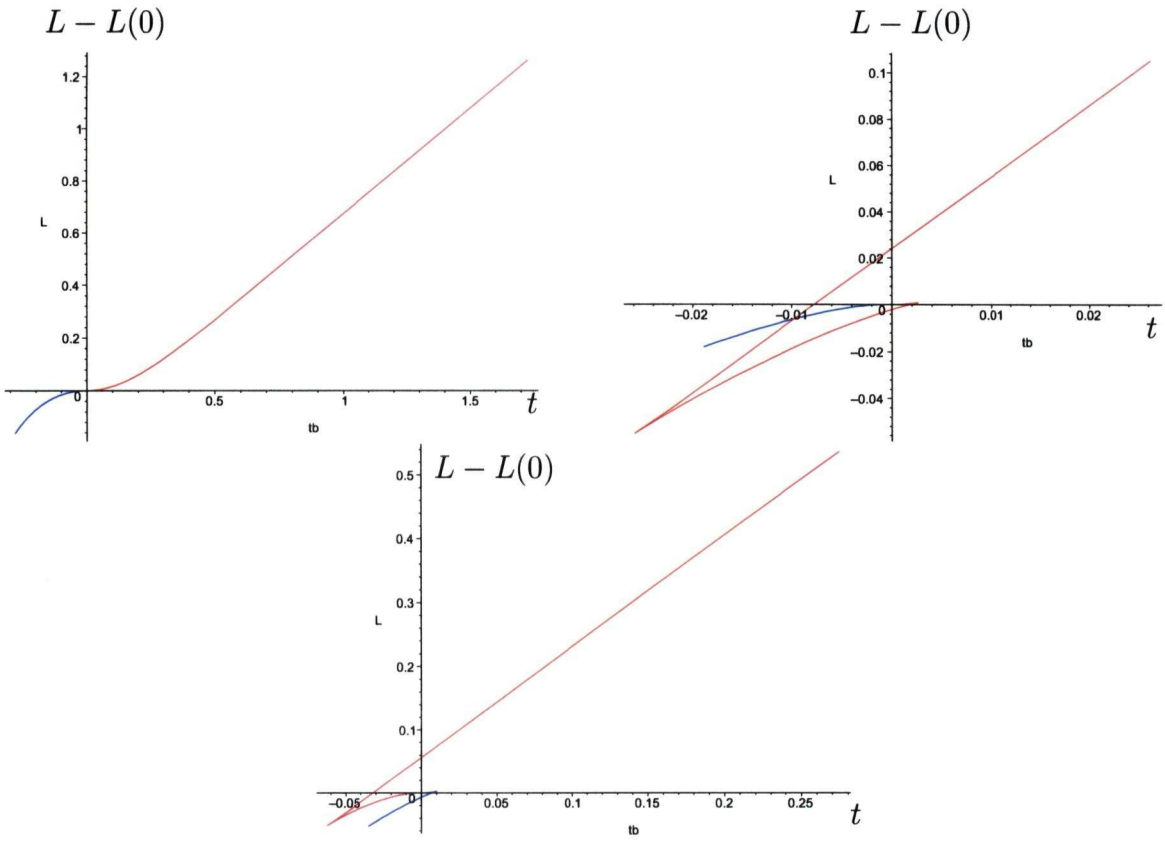

Figure 4.10: **Several $L(t)$ graphs with different value sets of (x_-, x_+), including both real and complex geodesics.** The red curves show the real geodesics, while the blue ones for the Euclidean. There exists a transition between a real geodesic and a Euclidean one at origin. For fixed parameters (x_-, x_+), it seems the number of geodesics should be conserved. From left to right, from top to bottom, the parameters are $(x_-, x_+) = (1, 2), (0.5, 4)$ and $(0.2, 1.25)$.

far from extremality we are expected to reproduce only the features of the finite mass black hole. The simplest scenario is that the real geodesics dominate the behavior of the correlation function both at early and late times.

On the other hand, one may worry that some change of behaviour (such as crossing of anti-Stokes lines) can occur at finite t_L, causing the real geodesic we are interested in to be subdominant at late times. This is a subtle question which we do not have a general answer for. However, we observe that for some black hole parameters, and for some region of boundary times, there are multiple *real* geodesics connecting the same boundary points. As we are interested mainly in the late time geodesics and their perturbations, we will concentrate on such black holes which do not exhibit this behaviour. As we have seen, those are the black holes which are close enough to being extreme.

For large enough boundary time, there is always a unique geodesic connecting the boundary points. As we decrease the value of the boundary time, there is a critical time t_{crit} (and corresponding energy E_{crit}) for which additional geodesics appear. This is seen in the right-hand plot of figure 4.5, for the case of a black hole far enough from extremality.

4.3 Charged Correlation Functions

We now discuss correlation functions of charged operators. As the analytic expressions are significantly more involved, we confine ourselves to discussing the qualitative features of the correlators, which are fairly similar to the neutral case discussed above.

To approximate correlators of operators which carry R-charge, we need to discuss trajectories of electrically charged particles[11]. We will only consider radial motion here, the addition of angular momentum having much the same effect as in the uncharged case[12]. The Lagrangian describing such a particle with charge q and unit mass is

$$\mathcal{L} = \frac{1}{2} g_{\mu\nu} \dot{X}^\mu \dot{X}^\nu + q A_\mu \dot{X}^\mu = \frac{1}{2}\left(-f(r)\dot{t}^2 + \frac{\dot{r}^2}{f(r)}\right) - \frac{\mathcal{Q}}{r^2}\dot{t} \tag{4.60}$$

where we have defined $\mathcal{Q} = cqQ$.

The worldline Hamiltonian $\mathcal{H} = (-f(r)\dot{t}^2 + f^{-1}(r)\dot{r}^2)/2$ is conserved, since the action is time translation invariant on the worldline. As we are interested in spacelike paths we can rescale λ to set $\mathcal{H} = 1/2$. The equations of motion are then

$$\dot{t} = \frac{1}{f(r)}\left(E - \frac{\mathcal{Q}}{r^2}\right), \qquad \dot{r}^2 = \left(E - \frac{\mathcal{Q}}{r^2}\right)^2 + f(r). \tag{4.61}$$

Note that shifting A_t by a constant (denoted in section 1 by Φ), which is just a gauge transformation, uniformly shifts the energy of all trajectories. This gauge freedom was fixed above, so that A_t vanishes at the outer horizon. We choose here to absorb the constant part of A_t, into the definition of E.

The relations following from (4.61) are as follows. First, the (real part of) the boundary time, for symmetric trajectories, is

$$t_0 = \int_{r_E}^{\infty} \mathrm{d}r \frac{(E - \frac{\mathcal{Q}}{r^2})}{V(r)\sqrt{(E - \frac{\mathcal{Q}}{r^2})^2 - V(r)}} \tag{4.62}$$

where r_E is the turning point described below. The length of the corresponding trajectory is given by

$$L = 2\int_{r_E}^{r_{\max}} \frac{\mathrm{d}r}{\sqrt{(E - \frac{\mathcal{Q}}{r^2})^2 - V(r)}} \tag{4.63}$$

where $r_{\max}$ is the long distance bulk cutoff introduced in section 3.

The equation for $r(\lambda)$ given in (4.61) cannot be interpreted as describing a particle with energy E^2 moving in a potential $V(r)$, since now the potential itself depends on E.

[11] Such particles exhibit interesting phenomena such as Schwinger pair production and induced emission [34]. See, e.g., [35] and, for a recent discussion, [36]. The Schwinger effect in curved space is studied in [37].

[12] As in that case, for an arbitrarily small angular momentum, one can find trajectories probing the region beyond the Cauchy horizon, but they return to a copy of the boundary on the same side of the Penrose diagram. These are therefore irrelevant to the two-sided correlators discussed here, and more generally we expect such trajectories not to dominate any gauge theory correlator.

However, one can still describe the qualitative features of the trajectory, which now depend on both the parameters $\mathcal{Q}$ and E.

The turning point, r_E, of the trajectory is the largest root of the equation

$$\left(E - \frac{\mathcal{Q}}{r^2}\right)^2 - V(r) = 0. \tag{4.64}$$

To visualise the situation, in figure 4.11 we plot $V(r) = -f(r)$ and the (positive semi-definite) function $(E - \mathcal{Q}/r^2)^2$, the behaviour of which depends on the sign of $\mathcal{Q}/E$. We therefore plot the function for both signs.

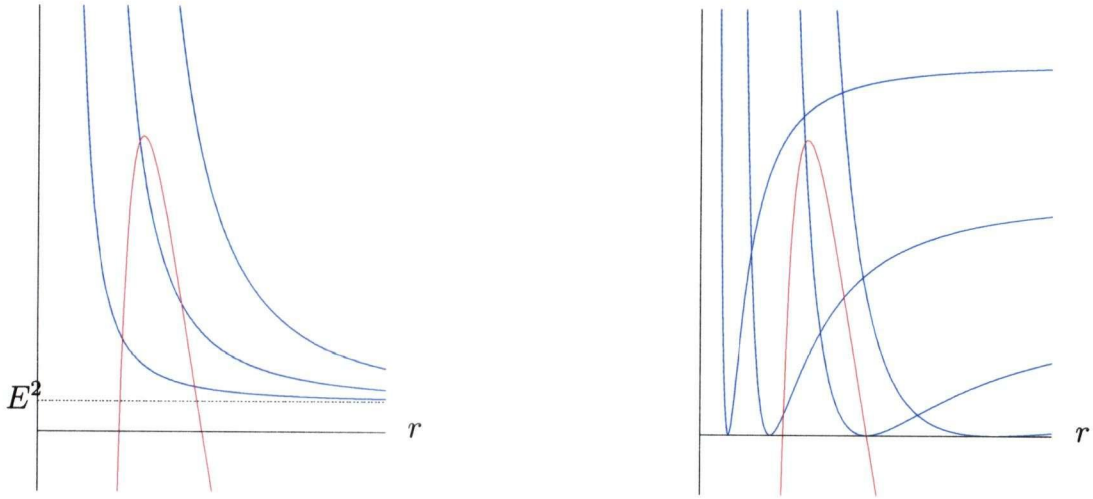

Figure 4.11: **The energy and effective potential for the spacelike geodesics of a charged probe particle.** The left-hand plot has $\mathcal{Q}/E < 0$. $V(r) = -f(r)$ is in red and $(E - \mathcal{Q}/r^2)^2$ in blue. Three trajectories with the same energy, E^2, but different charges, are shown. The right-hand plot has $\mathcal{Q}/E > 0$, and shows four trajectories with various values of the parameters. One has $\mathcal{Q}/E > r_+^2$ without a radial turning point, one has $\mathcal{Q}/E = r_+^2$ and two have $\mathcal{Q}/E < r_-^2$, one with a radial turning point and one without.

In either case, there are three possibilities:

- The graphs do not intersect, and there is no classical turning point. These classical trajectories end at the singularity.
- The graphs intersect twice, in which case the turning point is that intersection with the largest value of r. As in the uncharged case, this will always be in the region between the inner and outer horizons.
- The borderline case, in which there is a single intersection point, now not necessarily at precisely the top of the potential. Similar to the discussion above, looking at the behaviour of (4.62) and (4.63) near r_E reveals logarithmic divergences both in the boundary time and in the proper proper length of the geodesics. Therefore this value of E should be viewed as a limiting value, trajectories with larger value of E being irrelevant for our purposes.

These features of $r(\lambda)$ are similar to those discussed previously. It is clear that only those trajectories with a radial turning point will return to a boundary, but it is not clear which boundary this will be. To determine which trajectories are relevant for our two-sided correlators, we must also consider the behaviour of $t(\lambda)$, which is more involved than in the uncharged case. Let us take $E > 0$ so that t increases with affine parameter from the initial boundary[13]. Then, for $\mathcal{Q} < 0$ (the particle having a charge of opposite sign to the black hole), $\dot{t}$ just depends on the sign of the function $f(r)$: for $r > r_+$ it is positive, whereas for $r_- < r < r_+$ it is negative. So, if such trajectories have a radial turning point, and they do for small enough $\mathcal{Q}$, then they *will* connect the two boundaries of interest. In this case the coordinate $t(\lambda)$ is similar to the neutral geodesics.

The situation for $\mathcal{Q} > 0$ (the particle having a charge of the same sign as the black hole), is more complicated. The behaviour depends on the magnitude of $\mathcal{Q}/E$, and in each case is given by inspection of the right-hand side of the equation for $t(\lambda)$ in (4.61):

- For $\mathcal{Q}/E > r_+^2$, there is some $r > r_+$ for which $\dot{t} = 0$, and the trajectory will start to move backward in coordinate time before reaching the outer horizon. It crosses the event horizon, upon which it moves forward in coordinate time again. If such trajectories have a radial turning point (and some certainly do), then they will connect the two boundaries of interest.

- For $\mathcal{Q}/E = r_+^2$, $\dot{t} = 0$ precisely at the outer horizon, where the particle will necessarily have a radial turning point. It will then return to the same boundary, so such trajectories are of no concern to us.

- For $r_-^2 \leq \mathcal{Q}/E < r_+^2$, $\dot{t}$ does not vanish unless $r_- < r < r_+$. However, it necessarily has a radial turning point *before* the radius at which $\dot{t} = 0$, so will indeed connect the two boundaries of interest.

- Finally, for $\mathcal{Q}/E < r_-^2$, the particle may or may not have a radial turning point. If it does, then it will connect the boundaries of interest. Otherwise, the sign of $\dot{t}$ will flip at some $r < r_-$, and the trajectory will always hit the singularity.

The qualitative behaviour of the charged trajectories which do connect the two boundaries is thus similar to the neutral spacelike geodesics analysed above. They never cross the Cauchy horizon and, again, only reach a radius strictly larger than r_-.

4.4 Scanning Behind the Horizon

4.4.1 Perturbing the AdS-RN Spacetime

When the charged black hole is perturbed, linearised analysis suggests strong back-reaction near the inner horizon [21, 22, 23]. This is one instance of physics behind the horizon which would be nice to interpret in the gauge theory. We take here some preliminary steps towards this goal, postponing a more complete discussion for [29].

[13]Trajectories with $E < 0$, but the same sign of $\mathcal{Q}/E$, will just be mirror images of the trajectories we consider.

First, if one restricts attention to null perturbations which are either purely ingoing, or purely outgoing[14] (i.e., they are chiral in the sense of [38]), then one can solve for the perturbed metric exactly [28, 29]. One obtains an AdS version of the charged Vaidya solution [28, 39]. This solution contains one arbitrary function (the mass function) which depends on the profile of the perturbation. That profile can be varied, and can be arbitrarily localised[15]. By investigating the two-sided correlators (and other observables) as a function of the perturbation, one obtains an efficient method of scanning (at least some of) the region behind the horizon. We will demonstrate here the effects on our observables of a simple wave profile, that of an infinitely localised delta function pulse.

Secondly, in the asymptotically flat case, when both types of null perturbations are turned on[16] the spacetime is drastically changed near the inner horizon, resulting in the phenomenon of *mass inflation* [28]. We expect that this phenomenon persists in the asymptotically AdS case [29, 40]. We further expect that the dependence of some gauge theory observables will be non-analytic as a function of the perturbation strength: taking that strength to be arbitrarily weak does not diminish its effect.

Such non-analytic behaviour is not uncommon in field theories, and results from the existence of infra-red divergences. When re-summing perturbation theory, one discovers non-analytic dependence on coupling constants. Such behaviour would be slightly surprising for gauge theory on a compact space (a three-sphere in this case), at finite temperature and density, but it may be sensible in the infinite N limit.

Here, we find a behaviour which is perhaps more sensible. As we saw above the spacelike geodesics accumulate at some finite distance from the Cauchy horizon. This is no longer necessarily true of the perturbed geometry. Nevertheless the geodesics we investigate seem to always be screened from the dramatic behaviour at the Cauchy horizon, as is demonstrated below. It is unclear if this is a property of the particular observables we are studying, or a more general property of the gauge theory.

An Asymptotically AdS Charged Vaidya Solution

The Vaidya solution [39] describes an ingoing or outgoing null shell of matter incident on a vacuum black hole. Poisson and Israel generalised this to include charge in [28], their aim being to investigate the properties of the Cauchy horizon of the asymptotically flat Reissner-Nordström black hole. It is easy to further generalise these solutions to the asymptotically AdS case. In fact, though we will not do this here, one can derive [29] asymptotically AdS versions of the solutions relevant to mass inflation [28], describing both ingoing and outgoing flux.

In terms of the lightcone coordinate $u = t - r_*$ defined in section 2, the outgoing solution, in the region $r_- < r < r_+$, has the metric

$$ds^2 = -f(u,r)du^2 - 2dudr + r^2 d\Omega_3^2 \tag{4.65}$$

[14]For a massless field in AdS space, there are two types of perturbations, the non-normalisable one goes to a constant near the boundary. These are the type of perturbations we consider here. In the gauge theory this corresponds to turning on a marginal perturbation, with a specific time-dependent profile.

[15]This arbitrariness is similar to gravitational plane waves which solve Einstein's equation for an arbitrary wave profile.

[16]These are still not generic perturbations, so cosmic censorship considerations do not apply.

where all the u-dependence in the metric function is through that of the mass function $M(u)$:

$$f(u,r) = 1 - \frac{M(u)}{r^2} + \frac{Q^2}{r^4} + r^2. \tag{4.66}$$

The u-dependence is set by the flux sent in from the left-hand boundary, which must have the null energy-momentum tensor, whose only non-zero component is

$$T_{uu} = \frac{1}{2}\frac{\partial_u M(u)}{r^3}. \tag{4.67}$$

It is easy to check that this metric and energy-momentum tensor, together with the background gauge field given in (4.1) solve the five dimensional Einstein-Maxwell field equations with negative cosmological constant.

A Simple Example

The simplest case, which we will consider here, is to take

$$M(u) = m_1 + \Theta(u - u_p)\Delta m. \tag{4.68}$$

The corresponding energy-momentum tensor

$$T_{uu} = \frac{\Delta m}{2}\frac{\delta(u - u_p)}{r^3} \tag{4.69}$$

corresponds to an infinitely thin shell of null matter, the flux leaving the left-hand boundary at $t = t_p$. The spacetime splits into two regions: for $u < u_p$ the mass is m_1 and for $u > u_p$, the mass is $m_2 = m_1 + \Delta m$. We can then apply the previous analysis to the two regions, each with its own potential, and match across the $u = u_p$ surface. For non-rotating neutral geodesics the potential in each region is simply $V(r) = -f_{m_{1,2}}(r)$, where $f_m(r)$ is the radial function (4.66) with specific value of the mass parameter m.

If we take $\Delta m > 0$, then $f_{m_2} < f_{m_1}$ for all values of r. The roots $x_-(m_2)$ and $x_+(m_2)$ of f_{m_2} will thus be respectively less than $x_-(m_1)$ and greater than $x_+(m_1)$. The resulting geometry is shown schematically in figure 4.12.

Now, to see the effect of the perturbation on the gauge theory, consider again the two-sided correlator in the geodesic approximation. The perturbation is then encoded in properties of spacelike geodesics which intersect the surface $u = u_p$. Some possible geodesics are shown schematically in figure 4.12, in which we denote the intersection point by r_I, t_I. The interaction with the flux will change the path of the geodesic beyond this intersection point. We are only interested in those geodesics which intersect the flux in the region beyond the outer horizon and it is clear that late-time correlators will be most suitable.

As we change the time t_p at which the pulse leaves the boundary, the intersection point will change, and so will the length L of any geodesic. We should thus be able to see how the correlator changes as a function of t_p, a clear signal of physics behind the horizon. We demonstrate here how the information about the perturbation can be detected in our simple example.

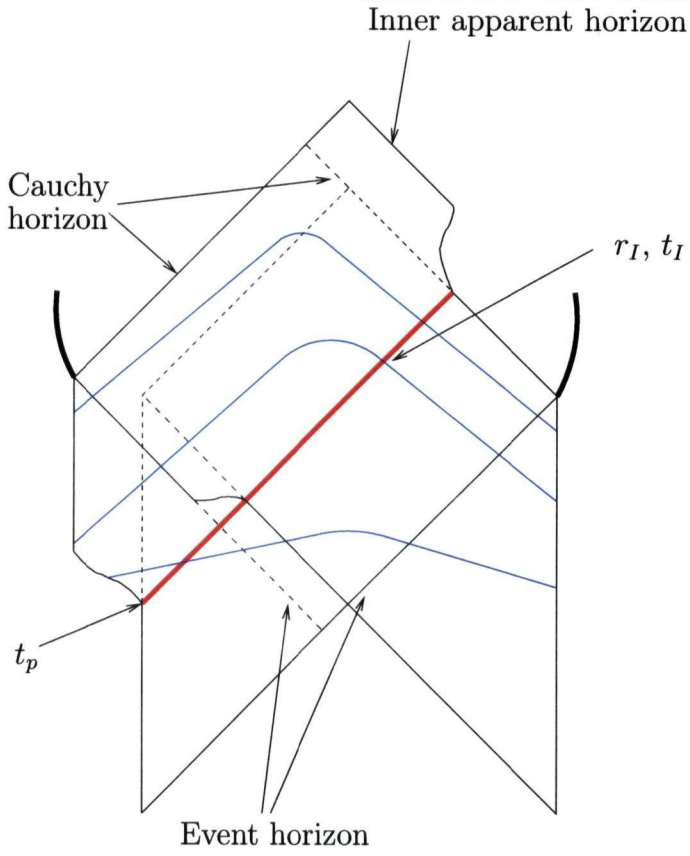

Figure 4.12: **The geometry of the perturbed spacetime, showing the event horizon, the Cauchy horizon and the inner apparent horizon.** The perturbation leaves the left-hand boundary at $t = t_p$, and is shown as a solid red line. Spacelike geodesics are shown schematically in blue, the point at which they interact with the perturbation being shown as r_I, t_I.

The only subtlety[17] is that the energy of the geodesics is no longer conserved as they cross the null shell. In the first region, from the metric (4.65), the conserved quantity is

$$E = -\frac{1}{2}\frac{\partial L}{\partial \dot{u}} = f(r)\dot{u} + \dot{r} \tag{4.70}$$

which is equal to the conserved energy $E = -\frac{1}{2}\frac{\partial L}{\partial \dot{t}}$ in the t, r coordinates we have been using for the unperturbed geometry. In the perturbed case, however, E is no longer conserved: if we define $E \equiv f(r,u)\dot{u} + \dot{r}$ then, from the geodesic equations,

$$\frac{\mathrm{d}E}{\mathrm{d}\lambda} = \frac{1}{2}\partial_u f(r,u)\dot{u}^2 \tag{4.71}$$

which, for the mass function as in (4.68), gives

$$\mathrm{d}E = -\frac{1}{2}\frac{\Delta m}{r^2}\delta(u - u_p)\,\dot{u}\,\mathrm{d}u. \tag{4.72}$$

Whereas the "energy" E is discontinuous across the null shell, the momentum normal to

[17] As pointed out to us by Simon Ross.

the shell, which is just $p_\perp = \dot{u}$, *is* continuous at the interaction point [41]. We can thus integrate the above equation, taking $\dot{u} = \dot{u}(m_1)$, the value of the momentum in the region with mass m_1. From the definition of E, and using the Lagrangian constraint $\mathcal{L} = 1$ for spacelike geodesics, we have

$$\dot{u} = \frac{E}{f(r,u)}\left(1 \pm \sqrt{1 + \frac{f(r,u)}{E^2}}\right), \tag{4.73}$$

so that

$$E_2 - E_1 = -\frac{1}{2}\frac{\Delta m}{r_I^2}\frac{E_1}{f_{m_1}(r_I)}\left(1 \pm \sqrt{1 + \frac{f_{m_1}(r_I)}{E_1^2}}\right) \tag{4.74}$$

where E_1 and E_2 denote the respective energies in the regions with mass m_1 and m_2. Note that $f(r_I, u_p) < 0$ so that $E_2 > E_1$.

4.4.2 Detecting the Perturbation

Qualitative Features

To analyse the qualitative properties of the geodesics, we re-consider the particle mechanics problem of section 3. The particle moves from the right-hand asymptotic region to the intersection point at $r = r_I$ in the effective potential $V_{m_1}(r) = -f_{m_1}(r)$, and with energy E_1. After the intersection point, the particle continues on its motion, but now in the effective potential $V_{m_2}(r) = -f_{m_2}(r)$, and with energy E_2. The various possibilities are shown in figure 4.13, in which we fix the energy of the geodesic, and vary the mass, which in turn changes the potential. We can vary the intersection point by varying t_p. There are then three possibilities (we will assume that the particle continues its motion entirely in V_{m_2} after the intersection, i.e. that it does not intersect the pulse a second time):

- If the intersection point satisfies $r_I > r_E(m_2)$, the turning point of the motion in $V_{m_2}(r)$, then the particle continues its motion in the modified potential until reaching the new turning point $r_E(m_2)$, and will thus still return to the opposite boundary. This is shown in the left-hand plot in figure 4.13.

- The centre plot has $r_I < r_E(m_2)$, so that after the interaction, it seems that the particle would be moving *below* $V_{m_2}(r)$. However, the new energy in the second region is $E_2 > E_1$, and this shift in the energy across the null pulse is sufficient to cause the particle to jump back above the second potential (we have checked that the shift in energy is large enough for a range of black hole parameters). This case is thus qualitatively similar to the previous one.

- The right-hand plot shows two ingoing particles, both with $E_1^2 > V_{\max}(m_1)$, so they would have fallen into the singularity in the unperturbed case. Here, however, they still have $r_I > r_E(m_2)$, so will continue their motion until reaching this turning point. Contrary to the unperturbed case, such geodesics will thus return to the opposite boundary.

The last case is interesting, since the trajectories now seem to cross the Cauchy horizon. However, as shown schematically in figure 4.12, by studying the trajectories more carefully one can see that this does not really happen. The trajectories cross the left-hand branch of the surface $r_-(m_1)$, which would have been the Cauchy horizon in the unperturbed spacetime, but is not in the perturbed case. The geodesics never cross the surface $r_-(m_2)$, which is the left-hand branch of the Cauchy surface in this case. Once again, it seems that the correlators are geometrically protected from the catastrophic instability of the Cauchy horizon.

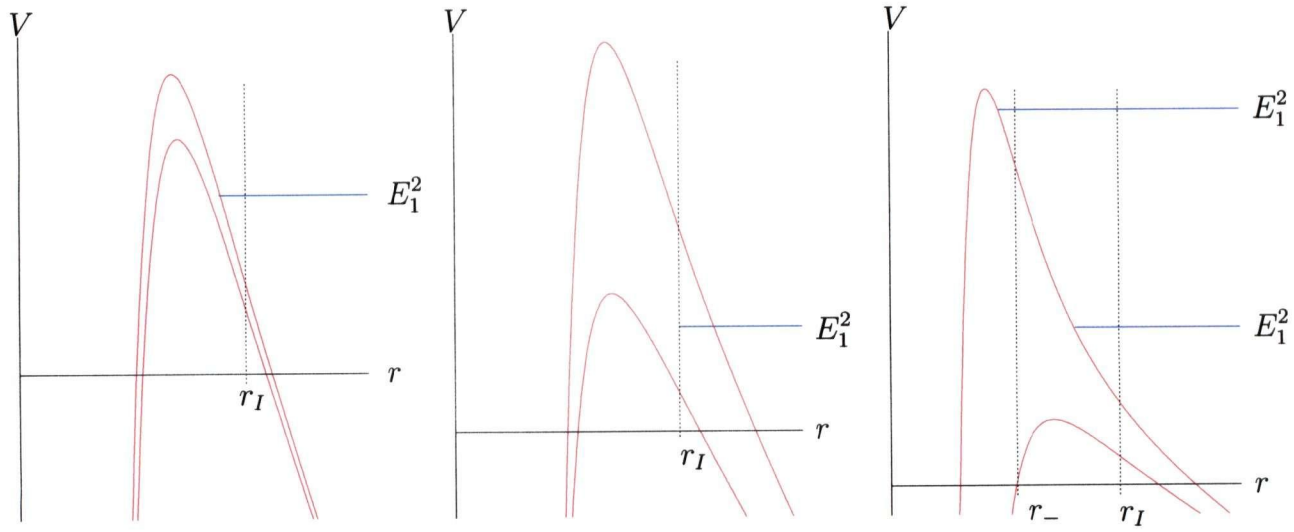

Figure 4.13: **The effective potentials before and after the perturbation, which make much difference for various values of energy.** The particles with energy E_1^2 are initially moving in the smaller potential, $V_{m_1}(r)$. They interact with the perturbation at some $r = r_I < r_+(m_1)$, inside the outer horizon, at which point the energy jumps to $E_2^2 > E_1^2$, and they continue to move in the larger potential, $V_{m_2}(r)$. The various possibilities shown are discussed in the text.

To demonstrate the scanning process of the region behind the event horizon, we will study the features of geodesics which fall into the first class discussed above, those with $E_1^2 < V_{\max}(m_1)$ which intersect the flux at $r_I > r_E(m_2)$. Such geodesics connect both boundaries of the perturbed spacetime, and therefore dominate the correlation functions of the perturbed gauge theory.

A Quantitative Plot of the Correlators

It is difficult to solve analytically for the behaviour of the correlator in the perturbed spacetime. Instead we demonstrate the process by numerically plotting the length of the geodesic as a function of t_p, the time of the perturbation.

Specifically , we plot here the fractional change in the length of the geodesic as a function of t_p,

$$\delta L = \frac{L(\Delta m) - L(\Delta m = 0)}{L(\Delta m = 0)}. \tag{4.75}$$

The method to generate the plot is not entirely obvious, so we outline it before presenting the result.

We first fix the initial roots, $x_\pm(m_1)$, of the potential $V_{m_1}(r)$, which fixes the initial mass m_1 and the charge (which remains unchanged). We fix Δm, the strength of the perturbation, which fixes the final mass m_2, and also the new roots $x_\pm(m_2)$ of the potential $V_{m_2}(r)$. Finally, we fix the initial energy E_1^2 of the geodesic in the unperturbed geometry, which fixes the boundary time of the correlator in that case. We take $E_1^2 \sim V_{\max}(m_1)$ to give late time geodesics, which should be guaranteed to interact with the perturbation in the relevant region.

In the unperturbed spacetime, with mass m_1, the geodesic with energy E_1^2 connects two specific points on opposite boundaries. The proper length of this approximates the correlator of operators inserted at these points. We need to compare this with the correlator in the perturbed spacetime, which *connects the same two points.* The correlators we compute before and after perturbing the spacetime should be the same; in the geodesic approximation, however, they are dominated by geodesics with different energies, say energy $\tilde{E}_1^2$ in the first region of the perturbed geometry (and, as discussed above, with a shifted energy $\tilde{E}_2^2$ in the second region).

Let us denote the points on the left- and right-hand boundaries which the geodesics connect as t_l and t_r. In the unperturbed spacetime, we have

$$t_l(m_1) + t_r(m_1) = 2E_1 \int_{r_{E_1}(m_1)}^{\infty} \frac{\mathrm{d}r}{V_{m_1}(r)\sqrt{E_1^2 - V_{m_1}(r)}}, \tag{4.76}$$

which can be computed as in subsection 3.2. This must be equal to the same quantity in the perturbed spacetime:

$$\begin{aligned} t_l(m_2) + t_r(m_1) = {} & \tilde{E}_1 \int_{r_{\tilde{E}_1}(m_1)}^{\infty} \frac{\mathrm{d}r}{V_{m_1}(r)\sqrt{\tilde{E}_1^2 - V_{m_1}(r)}} - \tilde{E}_1 \int_{r_{\tilde{E}_1}(m_1)}^{r_I} \frac{\mathrm{d}r}{V_{m_1}(r)\sqrt{\tilde{E}_1^2 - V_{m_1}(r)}} \\ & + \tilde{E}_2 \int_{r_{\tilde{E}_2}(m_2)}^{\infty} \frac{\mathrm{d}r}{V_{m_2}(r)\sqrt{\tilde{E}_2^2 - V_{m_2}(r)}} + \tilde{E}_2 \int_{r_{\tilde{E}_2}(m_2)}^{r_I} \frac{\mathrm{d}r}{V_{m_2}(r)\sqrt{\tilde{E}_2^2 - V_{m_2}(r)}} \end{aligned} \tag{4.77}$$

as can be seen by inspection of figure 4.12, and where $\tilde{E}_2$ is related to $\tilde{E}_1$ as in (4.74). Again, we can compute this in terms of elliptic integrals as in subsection 3.2. In the perturbed case the result is a function of the intersection radius r_I. Equating the two expressions for the boundary time (4.76,4.77) in principle gives then a relation $r_I(\tilde{E}_1)$. In practice, however, we need to know the interaction radius to compute $\tilde{E}_2$ (through (4.74)), which in turn we need to compute the interaction radius.

We can avoid this vicious circle by running through values of r_I (knowing that $r_+(m_1) > r_I > r_-(m_2)$) for each $\tilde{E}_1$, computing $\tilde{E}_2$ at each step (we take the smaller solution, with the negative sign in (4.74), to ensure $\tilde{E}_2^2 < V_{\max}(m_1)$), then comparing the two expressions (4.76,4.77) for these specific values. If they are close enough, then we know that we have the correct value for r_I. Numerical experiment for various values of the black hole parameters shows that the difference between the two expressions (4.76,4.77) for the boundary time is initially negative, for $r_I \sim r_+(m_1)$, and goes positive for $r_I \sim r_-(m_2)$. So we are guaranteed

a value of r_I for which the two expressions are identical, and we simply take that value for which they are closest.

We can use the resulting relation $r_I(\tilde{E}_1)$ to plot the proper length, L, and the time at which the spacetime is perturbed, t_p, as functions of $\tilde{E}_1$. The proper length of the geodesic in the perturbed spacetime is

$$L(\Delta m) = \int_{r_{\tilde{E}_1}(m_1)}^{\infty} \frac{\mathrm{d}r}{\sqrt{\tilde{E}_1^2 - V_{m_1}(r)}} - \int_{r_{\tilde{E}_1}(m_1)}^{r_I} \frac{\mathrm{d}r}{\sqrt{\tilde{E}_1^2 - V_{m_1}(r)}} + \int_{r_{\tilde{E}_2}(m_2)}^{\infty} \frac{\mathrm{d}r}{\sqrt{\tilde{E}_2^2 - V_{m_2}(r)}} + \int_{r_{\tilde{E}_2}(m_2)}^{r_I} \frac{\mathrm{d}r}{\sqrt{\tilde{E}_2^2 - V_{m_2}(r)}} \tag{4.78}$$

and the time t_p is

$$t_p = E_1 \int_{r_{E_1}(m_1)}^{\infty} \frac{\mathrm{d}r}{V_{m_1}(r)\sqrt{E_1^2 - V_{m_1}(r)}} - \tilde{E}_1 \int_{r_{\tilde{E}_1}(m_1)}^{\infty} \frac{\mathrm{d}r}{V_{m_1}(r)\sqrt{E_1^2 - V_{m_1}(r)}} + \tilde{E}_1 \int_{r_{\tilde{E}_1}(m_1)}^{r_I} \frac{\mathrm{d}r}{V_{m_1}(r)\sqrt{\tilde{E}_1^2 - V_{m_1}(r)}} - r_*(r_I) + r_*(\infty). \tag{4.79}$$

Both expressions can, again, be evaluated in terms of elliptic integrals as in section 3. Both L and t_p are functions of $\tilde{E}_1$, utilising the relation $r_I(\tilde{E}_1)$ found previously.

To recap, we run through values of $\tilde{E}_1$, then run through values of r_I at each step, computing $\tilde{E}_2$, and evaluating (4.76) and (4.77). We find a relation $r_I(\tilde{E}_1)$ by taking those values of r_I for which (4.76) and (4.77) are approximately equal, then evaluate L and t_p for each $\{\tilde{E}_1, r_I\}$. It is then a simple matter to plot the function $\delta L(t_p)$ as given in (4.75). The result is shown in figure 4.14. This schematic plot is for some specific values of the parameters ($x_- \sim 0.25, x_+ \sim 2.5$, which gives $m_1 = 10$ and $Q = 1.5$, $\Delta m = 0.5$ and $E^2 \sim 0.999 V_{\max}(m_1)$), but it seems to be representative of the general behaviour.

This plot demonstrates that our correlators are sensitive to a perturbation of the geometry which is localised beyond the outer horizon. We postpone further discussion for future work, and conclude by making a few comments.

First, we should note that figure 4.14 cannot be used for the region $V_{\max}(m_1) < \tilde{E}_1^2 < V_{\max}(m_2)$ of energies, since in this case the integrals have to be evaluated differently. Similar methods should work to generate a plot of $\delta L(t_p)$ for that range of energies however.

Moreover, we can only probe part of the region of the spacetime beyond the event horizon. There are no real solutions for r_I beyond a certain range of energies, and this range does not cover the entire region behind the event horizon.

Finally, it is intriguing that the plot of $L(t_p)$ in figure 4.14 is not single-valued. This means that there are two geodesics, with different energies $\tilde{E}_1$, which connect the fixed boundary points in the perturbed spacetime. Similar to the case of the unperturbed spacetime, this is reflected in some non-analytic behaviour of the correlators in the perturbed spacetime. It would be nice to get a better handle, through analytic calculations, on these

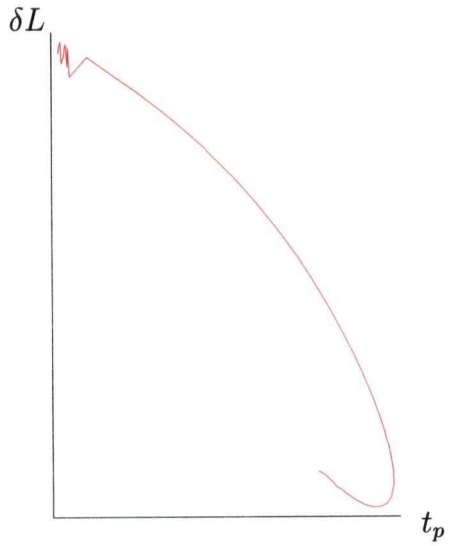

Figure 4.14: **Here we show the fractional change in the length of the geodesic as a function of t_p, for some choice of parameters as explained in the text.** The lack of smoothness for small t_p is due to numerical effects, and is not expected to be physical.

issues.

4.5 Conclusion and Prospect

Using AdS/CFT correspondence, we studied the charged black hole in 5 dimensional AdS space. The spacelike geodesics between two asymptotical boundaries dominate the correlation functions in the dual gauge theory. In general, the real geodesics are more important than the complex ones, different from Schwarzschild case. The correlators, as well as the related spacelike geodesics, are protected from Cauchy horizons, preserving the cosmic censorship principle.

Generally the inner horizon is unstable in perturbation, with a mass inflation arising near it. In our work, we turned a null outgoing perturbation pulse, and found some part of the Cauchy horizon was shifted. It is interesting to investigate the region very close to inner horizon, where dramatic behavior is supposed. We should check in that region whether the protection is still valid or not. Another interesting thing is the complex geodesics, which dominate at $t = 0$ in Schwarzschild case. We checked numerically that there are complex geodesics analytically continued from the real ones around the critical points, that is transition exists. So there are several questions we need to answer. Is the total number of geodesics including real and complex ones always conserved? In what region of parameters (x_-, x_+) are the complex geodesics more important? As showed in [9] sometimes the subdominated saddle point gives more important contribution, so in what sense can we rely on the geometric analysis? Furthermore, more discussion from the dual gauge theory point of view is very necessary.

We expect similar phenomena exist in rotating AdS black hole, however, that project maybe need more complicated analysis.

Appendix A

The Penrose Diagram

To work out the Penrose diagram, we need coordinates in which the boundary and singularity can be compared. Let us separate the space time into three regions: region A ($r < r_-$), region B ($r_- < r < r_+$) and region C ($r > r_+$). When in region A or C, we take

$$\mathrm{d}t = \frac{1}{2}(\mathrm{d}u + \mathrm{d}v) \tag{A.1}$$

and

$$u = t - r^*, \quad v = t + r^* \tag{A.2}$$

while in region B

$$\mathrm{d}t = \frac{1}{2}(\mathrm{d}u - \mathrm{d}v) \tag{A.3}$$

and

$$u = r^* + t, \quad v = r^* - t \tag{A.4}$$

so now the metric is

$$\begin{aligned} \mathrm{d}s^2 &= -f(r)\mathrm{d}u\mathrm{d}v, \quad \text{in region A or C} \\ &= f(r)\mathrm{d}u\mathrm{d}v, \quad \text{in region B} \\ &= -|f(r)|\mathrm{d}u\mathrm{d}v. \end{aligned} \tag{A.5}$$

Then continue the coordinates transformation, when in region A or C,

$$\begin{aligned} \tan U &= -e^{-\kappa_+ u} = -e^{-\kappa_+(t-r^*)} \\ &= -e^{-\kappa_+ t} e^{\kappa_+ x_0' \tan^{-1}(\frac{r}{r_0})} \left(\frac{|r-r_+|}{r+r_+}\right)^{1/2} \left(\frac{|r-r_-|}{r+r_-}\right)^{-\kappa_+\kappa_-/2}, \end{aligned} \tag{A.6}$$

$$\begin{aligned} \tan V &= +e^{+\kappa_+ v} = e^{\kappa_+(t+r^*)} \\ &= e^{\kappa_+ t} e^{\kappa_+ x_0' \tan^{-1}(\frac{r}{r_0})} \left(\frac{|r-r_+|}{r+r_+}\right)^{1/2} \left(\frac{|r-r_-|}{r+r_-}\right)^{-\kappa_+\kappa_-/2}, \end{aligned} \tag{A.7}$$

while in region B,

$$\begin{aligned} \tan U &= e^{\kappa_+ u} = e^{\kappa_+(t+r^*)} \\ &= e^{\kappa_+ t} e^{\kappa_+ x_0' \tan^{-1}(\frac{r}{r_0})} \left(\frac{|r-r_+|}{r+r_+}\right)^{1/2} \left(\frac{|r-r_-|}{r+r_-}\right)^{-\kappa_+\kappa_-/2}, \end{aligned} \tag{A.8}$$

$$\tan V = +e^{+\kappa_+ v} = e^{\kappa_+(r^*-t)}$$

$$= e^{-\kappa_+ t} e^{\kappa_+ x_0' \tan^{-1}(\frac{r}{r_0})} \left(\frac{|r-r_+|}{r+r_+}\right)^{1/2} \left(\frac{|r-r_-|}{r+r_-}\right)^{-\kappa_+\kappa_-/2}, \tag{A.9}$$

So we can get

$$\begin{aligned} \tan U \tan V &= -e^{2\kappa_+ x_0' \tan^{-1}(\frac{r}{r_0})} \left(\frac{|r-r_+|}{r+r_+}\right) \left(\frac{|r-r_-|}{r+r_-}\right)^{-\kappa_+\kappa_-}, \text{when in region A or C} \\ &= e^{2\kappa_+ x_0' \tan^{-1}(\frac{r}{r_0})} \left(\frac{|r-r_+|}{r+r_+}\right) \left(\frac{|r-r_-|}{r+r_-}\right)^{-\kappa_+\kappa_-}, \text{when in region B} \end{aligned} \tag{A.10}$$

which is analytic everywhere except at the inner horizon $r = r_-$. Obviously,

$$\begin{aligned} \text{when} \quad r \to +\infty, &\quad \tan U \tan V \to -e^{2\pi\kappa_+ x_0'} < -1, \\ r = r_+, &\quad \tan U \tan V = 0, \\ r = r_-, &\quad \tan U \tan V \to \infty, \\ r = 0, &\quad \tan U \tan V = -1, \quad \to \quad U = V + \frac{\pi}{2}. \end{aligned} \tag{A.11}$$

And the Penrose diagram is shown below

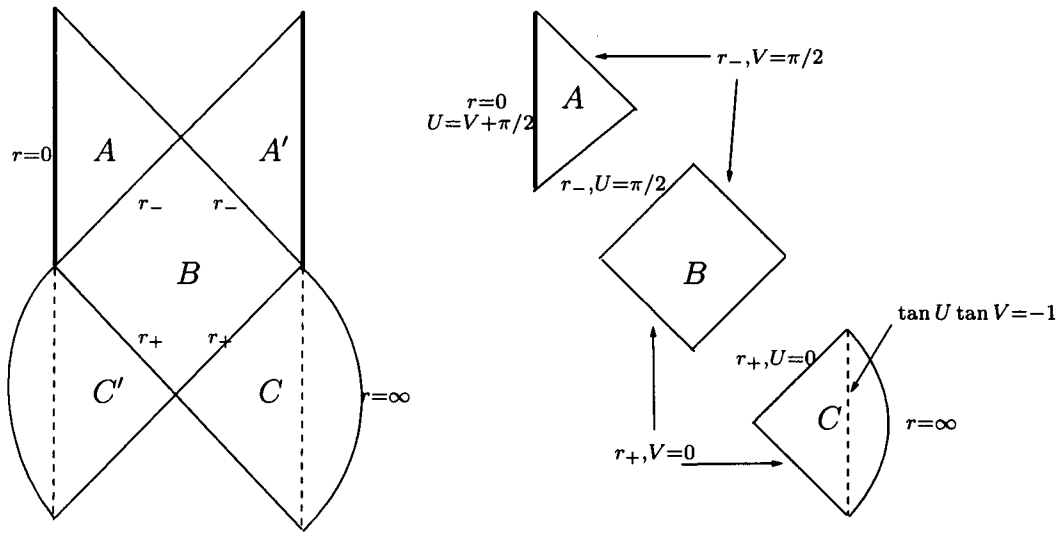

Figure A.1: **The Penrose diagram of the charged AdS black hole.** Using different Kruskal-like coordiantes for region A, C and B, we can get a general metric for the whole spacetime. Drawing the $r = 0$ singularity vertical, the boundaries have to be bowed out, while the 45 degree lines in the diagram are horizons.

In the figure, the singularity $r = 0$ is vertical and the boundary $r = +\infty$ is bowed out. Alternatively we can use some conformal transformation to make the singularity $r = 0$ is

bowed out while keeping the boundary vertical.

Make another coordinate transformation,

$$\tan U \to U, \qquad \tan V \to V, \tag{A.12}$$

the metric is thus

$$\mathrm{d}s^2 = \pm \frac{1}{\kappa_\pm^2} \frac{|f(r)|}{UV} \mathrm{d}U\mathrm{d}V, \tag{A.13}$$

where the $\pm$ sign corresponding to regions A and C, and region B respectively. The radial coordinate r in both cases is determined implicitly by

$$UV = \mp e^{2\kappa_+ x_0' \tan^{-1}(\frac{r}{r_0})} \left(\frac{r + r_+}{|r - r_+|}\right) \left(\frac{r + r_-}{|r - r_-|}\right)^{\kappa_+/\kappa_-}$$

which is analytic everywhere except at the inner horizon $r = r_-$. In the limits

$$r \to \infty \quad \Rightarrow \quad UV \to -e^{2\pi\kappa_+ x_0'} < -1, \tag{A.14}$$

$$r \to 0 \quad \Rightarrow \quad UV \to -1, \tag{A.15}$$

which is equivalent to (4.23) and gives the Penrose diagram.

Appendix B

The $t(E)$ Integral

Consider the integral (4.29) for non-rotating geodesics. Then $V(r) = -f(r)$ and, dropping the residue coming from integrating over the horizon, we have

$$-t_0 = \frac{E}{2}\int_{\tilde{x}_+}^{\infty} \mathrm{d}x \frac{x^{5/2}}{(x+x_0)(x-x_-)(x-x_+)\sqrt{(x+\tilde{x}_0)(x-\tilde{x}_-)(x-\tilde{x}_+)}}. \tag{B.1}$$

Defining a new variable t through

$$t^2 = a\left(\frac{x-\tilde{x}_+}{x-\tilde{x}_-}\right), \tag{B.2}$$

with a a constant to be determined, gives

$$-t_0 = \frac{E}{2}A\int_0^a \mathrm{d}t \left(1-\frac{\tilde{c}_0}{a}t^2\right)^{-1/2}\left(1-\frac{\tilde{x}_-}{a\tilde{x}_+}t^2\right)^{5/2}\left(\left(1-\frac{c_0}{a}t^2\right)\left(1-\frac{c_-}{a}t^2\right)\left(1-\frac{c_+}{a}t^2\right)\right)^{-1} \tag{B.3}$$

where we have set

$$A = \frac{2\tilde{x}_+^{5/2}}{a^{1/2}(\tilde{x}_+ + \tilde{x}_0)^{1/2}}\left((\tilde{x}_+ + x_0)(\tilde{x}_+ - x_-)(\tilde{x}_+ - x_+)\right)^{-1},$$

$$\tilde{c}_0 = \frac{\tilde{x}_- + \tilde{x}_0}{\tilde{x}_+ + \tilde{x}_0}, \qquad c_0 = \frac{\tilde{x}_- + x_0}{\tilde{x}_+ + x_0}, \qquad c_- = \frac{\tilde{x}_- - x_-}{\tilde{x}_+ - x_-}, \qquad c_+ = \frac{\tilde{x}_- - x_+}{\tilde{x}_+ - x_+}. \tag{B.4}$$

Now observe that

$$\left(\left(1-\frac{c_0}{a}t^2\right)\left(1-\frac{c_-}{a}t^2\right)\left(1-\frac{c_+}{a}t^2\right)\right)^{-1} = \hat{c}_0\left(1-\frac{c_0}{a}t^2\right)^{-1} + \hat{c}_-\left(1-\frac{c_-}{a}t^2\right)^{-1} + \hat{c}_+\left(1-\frac{c_+}{a}t^2\right)^{-1} \tag{B.5}$$

where

$$\hat{c}_0 = \frac{c_0^2}{(c_0-c_-)(c_0-c_+)}, \qquad \hat{c}_- = \frac{c_-^2}{(c_- - c_0)(c_- - c_+)}, \qquad \hat{c}_+ = \frac{c_+^2}{(c_+ - c_0)(c_+ - c_-)}. \tag{B.6}$$

If we take

$$a = \tilde{c}_0, \qquad k^2 = \frac{\tilde{x}_-}{\tilde{x}_+}\frac{1}{a}, \qquad \alpha_0^2 = \frac{c_0}{a}, \qquad \alpha_-^2 = \frac{c_-}{a}, \qquad \alpha_+^2 = \frac{c_+}{a}, \tag{B.7}$$

so that

$$\hat{c}_0 = \frac{\alpha_0^4}{(\alpha_0^2-\alpha_-^2)(\alpha_0^2-\alpha_+^2)}, \qquad \hat{c}_- = \frac{\alpha_-^4}{(\alpha_-^2-\alpha_0^2)(\alpha_-^2-\alpha_+^2)}, \qquad \hat{c}_+ = \frac{\alpha_+^4}{(\alpha_+^2-\alpha_0^2)(\alpha_+^2-\alpha_-^2)}, \tag{B.8}$$

then the integral becomes

$$-t_0 = \frac{E}{2}A\int_0^a \mathrm{d}t\sqrt{\frac{(1-k^2t^2)^5}{1-t^2}}\left(\frac{\hat{c}_0}{(1-\alpha_0^2t^2)}+\frac{\hat{c}_-}{(1-\alpha_-^2t^2)}+\frac{\hat{c}_+}{(1-\alpha_+^2t^2)}\right). \tag{B.9}$$

We now use

$$\sqrt{\frac{1-k^2t^2}{1-t^2}}\frac{1}{(1-\alpha^2t^2)} = \frac{(\alpha^2-k^2)}{\alpha^2}\frac{1}{(1-\alpha^2t^2)\sqrt{(1-t^2)(1-k^2t^2)}}+\frac{k^2}{\alpha^2}\frac{1}{\sqrt{(1-t^2)(1-k^2t^2)}} \tag{B.10}$$

and, noting that

$$\frac{\hat{c}_0}{\alpha_0^2}+\frac{\hat{c}_-}{\alpha_-^2}+\frac{\hat{c}_+}{\alpha_+^2} = 0, \tag{B.11}$$

we have

$$-t_0 = \frac{E}{2}A\int_0^a \mathrm{d}t\frac{(1-k^2t^2)^2}{\sqrt{(1-t^2)(1-k^2t^2)}}(I_0+I_-+I_+) \tag{B.12}$$

where

$$I_0 = \frac{\alpha_0^2(\alpha_0^2-k^2)}{(\alpha_0^2-\alpha_-^2)(\alpha_0^2-\alpha_+^2)}\frac{1}{(1-\alpha_0^2t^2)}, \tag{B.13}$$

$$I_- = \frac{\alpha_-^2(\alpha_-^2-k^2)}{(\alpha_-^2-\alpha_0^2)(\alpha_-^2-\alpha_+^2)}\frac{1}{(1-\alpha_-^2t^2)}, \tag{B.14}$$

$$I_+ = \frac{\alpha_+^2(\alpha_+^2-k^2)}{(\alpha_+^2-\alpha_0^2)(\alpha_+^2-\alpha_-^2)}\frac{1}{(1-\alpha_+^2t^2)}. \tag{B.15}$$

Each term can now be evaluated [31], to give

$$-t_0 = \frac{E}{2}A\left[\frac{k^6}{\alpha_0^2\alpha_-^2\alpha_+^2}\mathrm{F}(\phi,k)+\frac{(\alpha_0^2-k^2)^3}{\alpha_0^2(\alpha_0^2-\alpha_-^2)(\alpha_0^2-\alpha_+^2)}\Pi(\phi,\alpha_0^2,k)\right.$$

$$\left.+\frac{(\alpha_-^2-k^2)^3}{\alpha_-^2(\alpha_-^2-\alpha_0^2)(\alpha_-^2-\alpha_+^2)}\Pi(\phi,\alpha_-^2,k)+\frac{(\alpha_+^2-k^2)^3}{\alpha_+^2(\alpha_+^2-\alpha_0^2)(\alpha_+^2-\alpha_-^2)}\Pi(\phi,\alpha_+^2,k)\right] \tag{B.16}$$

where $\phi = \sin^{-1}a$. Substituting for the various constants gives the result (4.31) in the text.

Bibliography

[1] J. M. Maldacena, "The large N limit of superconformal field theories and supergravity," Adv. Theor. Math. Phys. **2**, 231 (1998) [Int. J. Theor. Phys. **38**, 1113 (1999)] [hep-th/9711200]; S. S. Gubser, I. R. Klebanov and A. M. Polyakov, "Gauge theory correlators from non-critical string theory," Phys. Lett. B **428**, 105 (1998) [hep-th/9802109]; E. Witten, "Anti-de Sitter space and holography," Adv. Theor. Math. Phys. **2**, 253 (1998) [hep-th/9802150].

[2] E. Witten, "Anti-de Sitter space, thermal phase transition, and confinement in gauge theories," Adv. Theor. Math. Phys. **2**, 505 (1998) [hep-th/9803131].

[3] O. Aharony, S. Gubser, J. Maldacena, H. Ooguri and Y. Oz, " Large N Field Theories, String Theory and Gravity", Phys. Rept. **323**, 183-386 (2000) [hep-th/9905111].

[4] H. Lin, O. Lunin and J. Maldecena, "Bubbling AdS Space and 1/2 BPS Geometries", JHEP **0410**, 025(2004) [hep-th/0409174].

[5] G. T. Horowitz and S. F. Ross, "Possible resolution of black hole singularities from large N gauge theory," JHEP **9804**, 015 (1998) [arXiv:hep-th/9803085].

[6] V. Balasubramanian and S. F. Ross, "Holographic particle detection," Phys. Rev. D **61**, 044007 (2000) [arXiv:hep-th/9906226].

[7] J. Louko, D. Marolf and S. F. Ross, "On geodesic propagators and black hole holography," Phys. Rev. D **62**, 044041 (2000) [arXiv:hep-th/0002111].

[8] V. E. Hubeny, "Precursors see inside black holes," Int. J. Mod. Phys. D **12** (2003) 1693 [arXiv:hep-th/0208047].

[9] L. Fidkowski, V. Hubeny, M. Kleban and S. Shenker, "The black hole singularity in AdS/CFT," JHEP **0402**, 014 (2004) [arXiv:hep-th/0306170].

[10] Dominic Brecher, Jianyang He and Moshe Rozali, "On Charged Black Hole in Anti-de Sitter Space," to be appeared in JHEP [arXiv:hep-th/0410214].

[11] J. M. Maldacena, "Eternal black holes in Anti-de-Sitter," JHEP **0304**, 021 (2003) [arXiv:hep-th/0106112].

[12] S. Hemming, E. Keski-Vakkuri and P. Kraus, "Strings in the extended BTZ spacetime," JHEP **0210**, 006 (2002) [arXiv:hep-th/0208003].

[13] P. Kraus, H. Ooguri and S. Shenker, "Inside the horizon with AdS/CFT," Phys. Rev. D **67**, 124022 (2003) [arXiv:hep-th/0212277].

[14] V. Balasubramanian and T. S. Levi, "Beyond the veil: Inner horizon instability and holography," hep-th/0405048.

[15] T. S. Levi and S. F. Ross, "Holography beyond the horizon and cosmic censorship," Phys. Rev. D **68**, 044005 (2003) [hep-th/0304150].

[16] J. Kaplan, "Extracting data from behind horizons with the AdS/CFT correspondence," hep-th/0402066.

[17] L. Fidkowski and S. Shenker, "D-brane instability as a large N phase transition," arXiv:hep-th/0406086.

[18] T. Hertog, G. T. Horowitz and K. Maeda, "Generic cosmic censorship violation in anti de Sitter space," Phys. Rev. Lett. **92**, 131101 (2004) [gr-qc/0307102]; T. Hertog, G. T. Horowitz and K. Maeda, "Negative energy in string theory and cosmic censorship violation," Phys. Rev. D **69**, 105001 (2004) [hep-th/0310054].

[19] M. Le Bellac, "Thermal Field Theory" (Cambridge University Press, 1996); A. J. Niemi and G. W. Semenoff, "Finite-Temperature Quantum Field Theory in Minkowski Space", Ann. Phys. **152, 105 (1984)**.

[20] G. Grignani, M. Orselli, G.W. Semenoff and D. Trancanelli, "The superstring Hagedorn temperature in a pp-wave background", JHEP **0306**, 006(2003)[arXiv:hep-th/0301186].

[21] R. Penrose, in "Batelle Rencontres," eds. C. De Witt and J. Wheeler (W. A. Benjamin, 1968).

[22] R. A. Matzner, N. Zamorano and V. D. Sanberg, "Instability of the Cauchy horizon of Reissner-Nordström black holes," Phys. Rev. D **19**, 2821 (1979).

[23] S. Chandrasekhar and J. Hartle, "On crossing the Cauchy horizon of a Reissner-Nordström black-hole," Proc. Roy. Soc. Lond. **A384**, 301 (1982).

[24] R. Penrose, "Gravitational Collapse: The Role Of General Relativity," Nuovo. Cim. **1**, 252 (1969) [Gen. Rel. Grav. **34**, 1141 (2002)]; R. Penrose, in "General Relativity, an Einstein Centenary Survey", eds. S. W. Hawking and W. Israel (Cambridge University Press, 1979).

[25] M. Dafermos, "Stability and Instability of the Reissner-Nordstrom Cauchy Horizon and the Problem of Uniqueness in General Relativity," gr-qc/0209052; M. Dafermos, "The interior of charged black holes and the problem of uniqueness in general relativity," gr-qc/0307013; M. Dafermos, "Price's law, mass inflation, and strong cosmic censorship," gr-qc/0401121.

[26] W. Israel, "Thermo Field Dynamics Of Black Holes," Phys. Lett. A **57**, 107 (1976).

[27] A. Chamblin, R. Emparan, C. V. Johnson and R. C. Myers, "Charged AdS black holes and catastrophic holography," Phys. Rev. D **60**, 064018 (1999) [hep-th/9902170]; A. Chamblin, R. Emparan, C. V. Johnson and R. C. Myers, "Holography, thermodynamics and fluctuations of charged AdS black holes," Phys. Rev. D **60**, 104026 (1999) [hep-th/9904197].

[28] E. Poisson and W. Israel, "Internal Structure Of Black Holes," Phys. Rev. D **41**, 1796 (1990).

[29] D. Brecher, J. He, M. Rozali and P. Saffin, Work in Progress.

[30] S. Chandrasekhar, "The Mathematical Theory of Black Holes" (Oxford University Press, 1985).

[31] P. F. Byrd and M. D. Friedman, "Handbook of Elliptic Integrals for Engineers and Physicists" (Springer-Verlag, 1954).

[32] V. Balasubramanian and P. Kraus, "A stress tensor for anti-de Sitter gravity," Commun. Math. Phys. **208**, 413 (1999) [hep-th/9902121].

[33] M. Abramowitz and I. A. Stegun, "Handbook of Mathematical Functions with Formulas, Graphs, and Mathematical Tables" (Dover Publications, 1965).

[34] G. W. Gibbons, "Vacuum Polarization And The Spontaneous Loss Of Charge By Black Holes," Commun. Math. Phys. **44**, 245 (1975).

[35] I. K. Affleck and N. S. Manton, "Monopole Pair Production In A Magnetic Field," Nucl. Phys. B **194**, 38 (1982); I. K. Affleck, O. Alvarez and N. S. Manton, "Pair Production At Strong Coupling In Weak External Fields," Nucl. Phys. B **197**, 509 (1982).

[36] M. Berkooz, B. Pioline and M. Rozali, "Closed strings in Misner space: Cosmological production of winding strings," JCAP **0408**, 004 (2004) [arXiv:hep-th/0405126].

[37] T. Friedmann and H. Verlinde, "Schwinger meets Kaluza-Klein," arXiv:hep-th/0212163.

[38] M. Berkooz, B. Craps, D. Kutasov and G. Rajesh, "Comments on cosmological singularities in string theory, JHEP **0303**, 031 (2003) [arXiv: hep-th/0212215].

[39] W. B. Bonnor and P. C. Vaidya, "Spherically Symmetric Radiation of Charge in Einstein-Maxwell Theory," Gen. Relativ. Grav. **1**, 127 (1970); B. T. Sullivan and W. Israel, "The Third Law of Black Hole Mechanics: What is it?," Phys. Lett. **79A**, 371 (1980).

[40] J. S. F. Chan and R. B. Mann, "Scalar wave falloff in asymptotically anti-de Sitter backgrounds," Phys. Rev. D **55**, 7546 (1997) [arXiv:gr-qc/9612026].

[41] C. Barrabès and W. Israel, "Thin shells in general relativity and cosmology: The lightlike limit," Phys. Rev. D **43**, 1129 (1991).